https://doi.org/10.5194/egusphere-2025-6539
Preprint. Discussion started: 12 January 2026

Ballistic projectile hazard of major explosions and paroxysms at Stromboli (Italy) with uncertainty quantification: 1. Mapping method and data analysis

Andrea Bevilacqua[1], Patrizia Landi[1], Paola Del Carlo[1], Augusto Neri[1], Massimo Pompilio[1]

[1] Istituto Nazionale di Geofisica e Vulcanologia, Sezione di Pisa, Pisa, 56125, Italy

Correspondence to: Augusto Neri (augusto.neri@ingv.it)

Abstract. This study presents a novel method to map the areas affected by ballistic fallout generated by major explosions and paroxysms at Stromboli as well as quantitative analyzes of these areas. The mapping method is based on a simplified description of the affected areas by a circular proximal area and up to three circular sectors with variable radius and width, and uncertainty based on expert judgement. The dataset of maps includes a total of 67 events over ≈150 years, based on an extensive review of historical, observational, and monitoring data. Our findings highlight that 12%-14% of major explosions can exceed 1,000 m, and 29% of paroxysms extend over 2,000 m of distance; (2) directional analysis of ballistic dispersal shows a predominant direction towards the East half-plane (87%) for major explosions and towards the North half-plane (64%) for paroxysms; (3) the average affected area was 6.9×10^4 m² for major explosions and 3.6×10^5 m² for paroxysms with a mean sector width of ≈90° for both categories. Notably, major explosions and paroxysms show a continuous distribution of maximum ballistic distance and area affected, suggesting the absence of a net separation between these two categories in terms of these products dispersal. Results highlight the limited influence of uncertainty in reconstructing the dispersal areas and stress the importance of volcanological monitoring. By quantifying distances, directions, and areas affected by ballistic fallout, we provide the necessary data, together with their uncertainty, to produce probabilistic maps of ballistic hazard presented in the companion study.

Short summary. This study investigates how far projectiles are thrown during major explosions and paroxysms at Stromboli volcano. The researchers analyzed 67 events spanning about 150 years to study the distances, directions, and areas affected by these projectiles, based on an extensive review of historical, observational, and monitoring data, and by using an innovative approach to map affected areas.

https://doi.org/10.5194/egusphere-2025-6539
Preprint. Discussion started: 12 January 2026

1 Introduction

Ballistic projectiles are centimeter to meter sized clasts, either juvenile or lithics, which are commonly ejected during explosive activity The clasts are large enough to follow nearly parabolic trajectories which are not significantly affected by the wind field (Blong, 1984). Several previous studies were focused on the volcanic hazard associated with ballistics (Alatorre-Ibargüengoitia et al., 2006, 2012, 2016; Rosi et al., 2013; Fitzgerald et al., 2014; Tsunematsu et al., 2016; Bernard, 2018). In fact, ballistics ejected during sudden explosions producing single or multiple directed blasts, are the most common cause of fatal accidents within a 5 km radius from active volcanoes and caused tens of casualties and hundreds of injuries in the past decades (Brown et al., 2017). They represent a major hazard at many active volcanoes in the world, in particular those that are sites of tourist attraction, e.g., Galeras (Colombia), Popocatepetl (Mexico), Yasur (Vanuatu), Tongariro (New Zealand), Ontake and Shinmoedake (Japan) (Maeno et al. 2013; Yamaoka et al, 2016; Fitzgerald et al., 2018) and Stromboli (Italy).

Stromboli island constitutes the ca. 3 × 4 km subaerial section of an active composite volcano, slightly elongated in the NE-SW direction and rising to an elevation of 924 m above sea level. The island is notable for a horseshoe-shaped depression called Sciara del Fuoco located in the NW part of the volcano. The ongoing volcanic activity generally occurs in multiple craters within a relatively flat region known as Crater Terrace, located at about 750 m elevation above the Sciara del Fuoco (Fig. 1i).

At Stromboli, the greater ballistic hazard is related to major explosions and paroxysms that interrupt the persistent mild strombolian activity of the volcano (Barberi et al., 1993; Pompilio et al., 2010; Bertagnini et al., 2011). The hazardous area affected by ballistic projectiles is a key observation and is commonly assumed as the main discriminant factor to distinguish between ordinary activity, major explosions and paroxysms (Barberi et al., 1993; Rosi et al., 2013; Bevilacqua et al., 2020b). This area is limited to the Crater Terrace and upper Sciara del Fuoco in case of ordinary activity, to the summit area of the volcano (up to a maximum distance of about 1 km from the vents) and Sciara del Fuoco during major explosions, and can extend down to low elevations along large part of the island, and sometimes beyond the shoreline (up to ca. 2.5 km), during the paroxysms.

The present early-warning systems at Stromboli are able to recognize precursor signals a few minutes before these explosive events, a time too short to find a safe shelter or escape from the hazard zone (Di Lieto et al., 2020; Ripepe et al., 2021; Insinga et al. 2025). In this context, quantitative assessments of the ballistic hazard at different sites of the island becomes a crucial means for any action of risk mitigation and emergency planning.

Estimates and robust statistics of distances, directions and areas affected by ballistic projectiles therefore represent key information to feed reliable hazard assessments. Stromboli offers observations of tens of explosive events in either the major explosions and paroxysms categories (Bertagnini et al., 1999; 2008; Coltelli et al., 2000; Rosi et al., 2006; Pistolesi et al.,

https://doi.org/10.5194/egusphere-2025-6539
Preprint. Discussion started: 12 January 2026

2011; Giordano and De Astis 2021; Andronico et al., 2021) and several illustrative examples of ballistics ejected during these events are shown in Figure 1 and Figure S1.

In this study, we performed a careful spatial analysis and uncertainty assessment using the data collected in two open INGV catalogs of major explosions and paroxysms at Stromboli (Bevilacqua et al., 2020a; Bevilacqua et al., 2023). Building on the two datasets we have developed a novel method to map the area affected by the fallout of ballistic projectiles in a remarkable number of events (a total of 67 events, i.e., 24 paroxysms and 43 major explosions) including the assessment of its uncertainty. The new method uses circular sectors with varying radii, angles and uncertainty ranges. Thank to this approach, we calculated the statistics of the radius, directional angle, and the extent of the area affected by ballistic projectiles.

To evaluate the effect of poorly constrained information on the distances and directions of past explosions, we utilize a doubly stochastic methodology, involving uncertain probabilities (Sparks & Aspinall, 2004; Marzocchi & Bebbington, 2012; Bevilacqua et al., 2015). Historical data are regarded as a random array, and we separately estimate this epistemic uncertainty from the statistical model for future distance, direction, and affected area (Bebbington, 2013; Bevilacqua et al., 2016; 2018; Richardson et al., 2017; Watson et al., 2017). Specifically, our calculations are conducted using Monte Carlo simulations that randomly perturb the simplified maps of past events. We present all our results as mean values along with the 5^{th} and 95^{th} percentile values (Neri et al., 2015; Bevilacqua et al., 2017; Rutarindwa et al., 2019; Tadini et al., 2022; Aravena et al., 2022; 2023).

These results enable a greater understanding of the hazard and ultimately risk of ballistics on Stromboli and represent the key information to produce probability hazard maps of ballistic projectiles from major explosions and paroxysms, or for both types of events considered together, as described in the companion study (Bevilacqua et al., submitted).

https://doi.org/10.5194/egusphere-2025-6539
Preprint. Discussion started: 12 January 2026

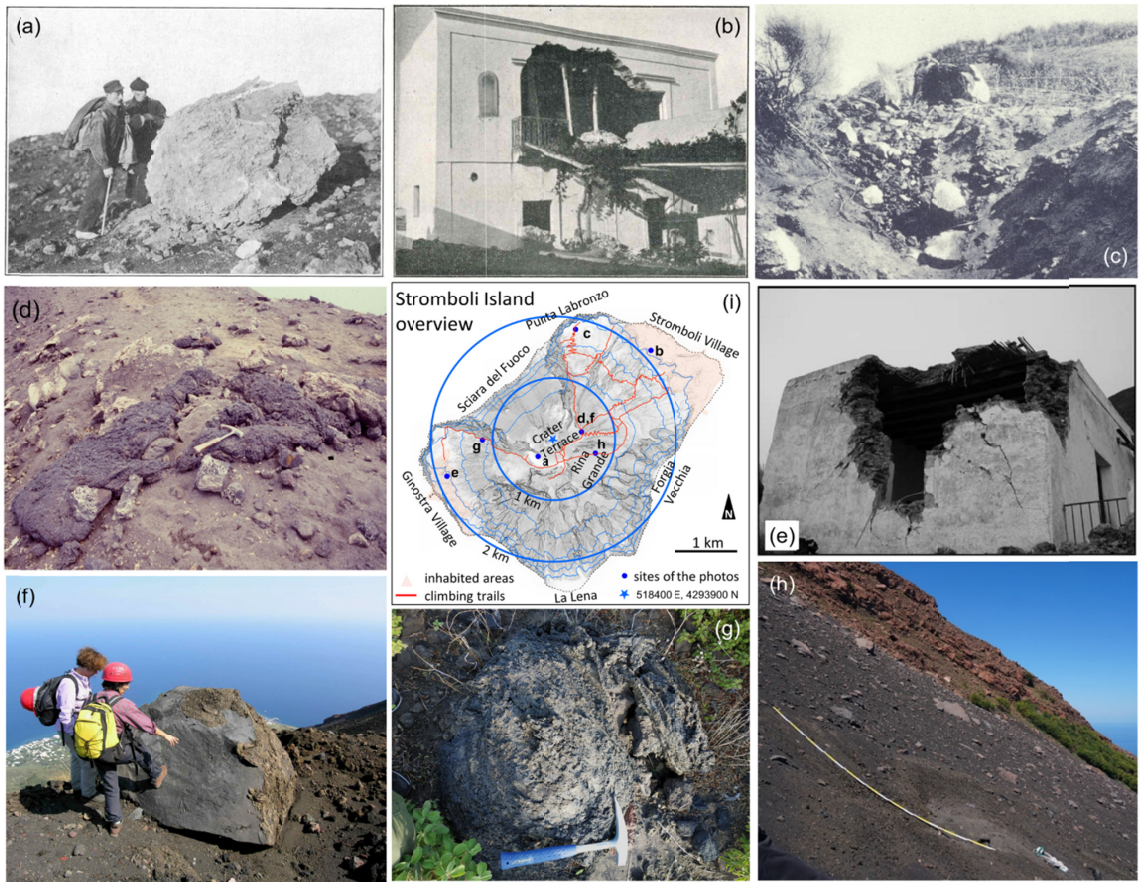

Figure 1: Examples of sizes and type of ballistic projectiles observed during past events at Stromboli. (a) conglomerate boulder ejected by the paroxysm of 26th Nov. 1915 (Perret, 1916); (b) house in S. Bartolo hamlet hit by a large ballistic projectile during the paroxysm of 22nd May 1919 (Ponte, 1924); (c) ballistic block impacted near Labronzo Lighthouse during the paroxysm of 11th Sept. 1930 (Rittmann, 1931); (d) flattened bomb ejected ca. 500 m from the craters by the major explosion of 8th Sept. 1998 (P. Landi ph.); (e) house in Ginostra village hit by a large ballistic projectile during the paroxysm of 5th April 2003 (Rosi et al., 2006); (f) large block ejected ca. 600 m from the craters during the paroxysm of 5th Apr. 2003 (courtesy of A. Bertagnini); (g) flattened bomb observed along Ginostra trail after the paroxysm of 3rd Jul. 2019 (A. Bevilacqua ph.); (h) impact crater found in Rina Grande area after the major explosion of 13th May 2022 (P. Landi ph.). The small map (i) indicates the sites of the photos.

https://doi.org/10.5194/egusphere-2025-6539
Preprint. Discussion started: 12 January 2026

2 Approach and Methods

Our analysis relies on the critical study of all available documentation of past events, fully reported in Bevilacqua et al. (2020a; 2023) and detailed in Section 3. In particular, we schematically mapped the area reached by ballistic projectiles by using circular sectors that envelope the areas affected by ballistic projectiles as deducted from the field reports, the surveillance cameras reports and the tele-photos. Sites of fire ignition, field observations made by the authors of this study, and witness testimonies, were useful complementary information.

The approach that we followed for mapping past ballistic distributions involved some assumptions and limitations:

(i) the projectile distribution is reconstructed based on all available ground and remote observations. No specific assumptions regarding the conditions of the explosive mixture at the source, nor any descriptive models of projectile dynamics, were used in the definition of the areas affected, although available knowledge on projectile dynamics in the literature was considered in defining the lower limit of the clast size (de'Michieli Vitturi et al., 2010; Vanderkluysen et al., 2012; Valentine et al., 2012; Taddeucci et al., 2013; 2017; Tsunematsu et al., 2015; Bertin, 2017; Massaro et al., 2022).

(ii) We focused on the maximum distances and dispersion directions concerning the potentially most dangerous projectiles, i.e., lithic and scoria clasts larger than about 5-10 cm in diameter. Smaller clasts and pumice fallout were not considered.

Our historical reconstructions do not quantify the spatial density of the projectiles, and exclusively describe the areas affected by ballistic fallout. The areal density distribution of the projectiles which is highly variable, e.g. up to 2 orders of magnitude depending on the distance from the crater (Gurioli et al., 2013; Breard et al., 2014; Bisson et al., 2023; Bevilacqua et al., 2024; Schmid et al., 2025), was not considered in this analysis, although it is important for impact assessments.

2.1 Reconstructing the areas affected by ballistics of past major explosions and paroxysms

Circular sectors approximately represent the areas affected by ballistics because this geometry mirrors, at a first order, the envelope of the trajectories of projectiles that are radially ejected from a central eruptive vent. Moreover, the great majority of the pre-existing maps were roughly shaped in that way. In fact, they consisted of one or more hand-drawn lobes enlarging further from the vents (Bertagnini et al., 1999; Rosi et al., 2006), open half-ovals (Andronico and Pistolesi 2010; Rosi et al., 2013), or arched isoline segments (Pistolesi et al. 2011; Giordano and De Astis 2021). A few pre-existing maps resembled ovals or irregular segments (Coltelli et al., 2000; Giordano and De Astis 2021) which we replicated by using a circular sector plus a proximal axisymmetric part, as described in the following sections.

However, this approximation is uncertain, and most pieces of information on ballistic dispersal are imprecise, for several reasons:

- named localities or trail paths lack of geographic coordinates;

https://doi.org/10.5194/egusphere-2025-6539
Preprint. Discussion started: 12 January 2026

- distance or altitude values are commonly expressed in multiples of 100 m;
- most recognizable projectiles are described but others could not be excluded nearby; as a consequence, a measurement of the spatial density of projectiles is rarely provided;
- ignited fires likely started by ballistic fallout are described but the actual ballistic source was not determined;
- access to the summit areas after the eruptions is limited to a few trails and depends on safety conditions, and observations are often carried out in haste and from a distance;
- observations from remote locations (e.g., villages) are affected by perspectival errors;
- distances and angles are not related to the vent ejecting the projectile but to a fixed center;
- observations are often collected days to months after the explosion has occurred.

Importantly, the number of projectiles per unit area was most of the times hard to evaluate, and therefore our reconstructions cannot be read in terms of isolines of projectile density or of ground cover percentage. Unobserved, broken, or unrecognized projectiles of small size are a significant limitation to such measurements. In fact, witnesses did not easily provide quantitative information, and, as a result, only the greatest or the most damaging projectiles are usually mentioned. As a consequence, in our estimates we focused on the areas affected by ballistic fallout with no information on the spatial density also due to this difficulty.

Depending on the accuracy and reliability of the information sources, we also assigned the past events to different "uncertainty classes" as detailed in the sequel. We classified the information of past events in three types:

- constraints on radial distance (radially affected areas);
- constraints on direction, only at low elevation (affected sectors);
- constraints on radial distance and direction (affected locations);
- pre-existing maps of affected area, possibly incomplete or incorporating lapilli fallout.

In Figure 2 we sketched examples of how these four types of information were utilized to draw circular sectors. By utilizing circular sectors, we assumed that if a location was affected by ballistics, also the segment between that place and the vents was considered affected. This assumption was conservative against possibly rolling and bouncing projectiles, but it also considered that the available records may have primarily reported the farthest projectiles from the eruptive vents, which determined an impact in the inhabited or frequented areas.

In Figure 2a we show an example constraint on radial distance, in all directions. In fact, to every major explosion and paroxysm we assumed that there is a minimum proximal circular area affected by ballistics, but some explosions were described to have been radially greater. This was a relatively uncommon type of constraint: only ca. 1/10 of major explosions and 1/6 of the paroxysms maps assumed such a larger circular area.

In Figure 2b we show an example constraint on sector direction at low elevation, assumed in mapping 2/3 of the paroxysms and not for major explosions. In fact, we know that some historical paroxysms affected a flank of the volcanic edifice, an

https://doi.org/10.5194/egusphere-2025-6539
Preprint. Discussion started: 12 January 2026

inhabited area, or its cultivated land, without further information. For 1/3 of the paroxysms this happened in the direction where the ballistics were observed farthest from the vents. In this case, a circular sector was defined in a way that the lateral sides enveloped the mentioned area (e.g., inhabited areas, cultivated lands, burned areas); its radius was left significantly uncertain (more details in Tab. 1, high uncertainty class).

In Figure 2c we show an example constraint on specific sites or areas. A circular sector enveloping the affected region is defined, centered on the center of Crater Terrace. When multiple observations of this type were made in different sites, separate sectors were distinguished if the distance was significantly different (with respect to a precision of 100 m). This is the most common type of information, available in 7/8 of the paroxysms, and 5/6 of major explosions.

In Figure 2d we show an example constraint based on a pre-existing map of ballistic dispersion. Only ca. 1/4 of paroxysms and of major explosions were previously mapped. Moreover, a clear distinction between ballistic fallout and wind-blown pumice lapilli fallout was not always detailed, and the ballistics dispersion was rarely mapped in all directions. In these cases, we followed a precautionary conservative approach, and fully enveloped the mapped area within the uncertainty buffer of one or more circular sectors.

2.2 Mapping of ballistic projectile distribution with uncertainty assessment

Our statistical analysis of distance and direction is expressed in polar coordinates, with the center located at 518400 E, 4293900 N, UTM WGS84, Zone 33N, that is approximately the center of the Crater Terrace. In fact, the involvement of distinct and/or multiple craters in the different events is not considered here and such variability is included in the radial uncertainty detailed below. Note that all vents are generally located within ca. 100-150 m from this center. In each simplified map, a proximal axisymmetric part was defined, followed by 1 to 3 circular sectors with greater distance ranges. Craters' architecture, possibly modified by the most intense explosions, as well as shielding obstacles and differences in elevation are possible factors in determining these asymmetric features, although at Stromboli these were mostly studied for smaller events than major explosions (e.g., Valentine et al., 2012; Taddeucci et al., 2013; Iezzi et al., 2023). The proximal axisymmetric part was a circle determined by just a radial distance and the circular sectors were characterized by radial distances, the azimuth angles of the bisector and the half-width angles. These measurements are all reported in Tables S1 and S2.

While we tailored these sectors as tight as possible on the existing data or the pre-existing maps, this in a few cases produced a slight enlargement, up to ca. 100 m for major explosions and 200 m for paroxysms, of the areas affected by the ballistic fallout. These uncertainties are consistent with the uncertainty classes defined in the sequel.

Three classes of uncertainty on radii and angles were considered: low uncertainty (just for the major explosions of which any maps of ballistic fallout were available), moderate uncertainty (for both the major explosions and the paroxysms of which

https://doi.org/10.5194/egusphere-2025-6539
Preprint. Discussion started: 12 January 2026

the ballistic fallout has been fully described all around the source), and high uncertainty (for some of the historical paroxysms that have weak constraints to the ballistic fallout in some directions).

In the low uncertainty class a uniform uncertainty between 0 and 100 m was assumed on all radial distances, equivalent to a mean enlargement of 50 m. In fact, our field experience led us to estimate within 100 m the accuracy of many of the past field observations missing geographical coordinates and the capability to recognize a ballistic bomb from distance. Moreover, this is also approximately the radial size of Crater Terrace, where all active vents are located.

In the moderate and high uncertainty classes the field observations on radial distance were not pinpointed to any specific modern reference site, and therefore we assumed doubled this uncertainty, i.e, we produced a mean enlargement of 100 m. Such distance uncertainty was also translated to an equivalent angular uncertainty by considering the length of circular arcs drawn at approximately the average maximum ballistic distance (i.e., ca. 700 m for major explosions and 1400 m for the paroxysms).

Finally, the high uncertainty class stood again for a mean enlargement of 100 m in each sector for which a specific distance value was available in literature, but, in addition, denoted greater uniform errors in the sectors where the lower portions of the island had been affected by ballistic projectiles, but no precise distance values were specified.

In general, we expressed the radial and the angular uncertainties as independent uniformly distributed variables, with a range of variability depending on the class of uncertainty of the corresponding event, as reported in Table 1.

In Figures 3 and S2 we describe a few illustrative examples of ballistics maps following the described strategy, showcasing the four typologies of data constraints described above and the three classes of uncertainty (low, intermediate, high); Supporting Texts S1 and S2 provide a complete description of all the 67 mapped events. We remark that, ultimately, this analysis process adopts expert judgment to transform diverse observational data into a dataset of simplified maps able to capture the first-order characteristics of the dispersal process. In doing this, we aimed at keeping things as simple as possible to maintain full transparency on our choices and ease the replicability of our maps and results.

2.3 Analysis of maximum distance, direction and area affected by ballistic projectiles

For each sector of each explosion, a Monte Carlo simulation is performed with respect to uncertainty sources, sampling independently the radial and angular uncertainties. This enables the production of doubly stochastic probability percentages, density functions, exceedance probability functions, all affected by uncertainty and expressed in terms of 5^{th}, mean and 95^{th} percentile values (Sparks & Aspinall, 2004; Marzocchi & Bebbington, 2012; Bevilacqua et al., 2015). We note that the random enlargement of the circular sectors can appropriately reduce the size of adjacent sectors defined over a different distance, if the latter is shorter.

In particular, for every distance threshold $d > 0$ m, the exceedance probability function of the maximum ballistic distances in all directions is calculated as:

https://doi.org/10.5194/egusphere-2025-6539
Preprint. Discussion started: 12 January 2026

$$F(d) = P\{ X > d \}, \quad \text{and} \quad X := D_{ij}, \tag{1}$$

where j is uniformly sampled in 1,…, N, and i is sampled among the number of sectors of explosion j-th, weighted in proportion to W_{ij} / 360°, where N is the total number of the explosions in the dataset and W_{ij} is the width of the sector. In this formula, the width of the axisymmetric part is defined as the complement to 360° of the union of all the sectors.

Similarly, for every angle θ in [0, 360°], the ballistic direction probability percentage is:

$$G(\theta) = |\{j : \theta \in \cup_i (\alpha_{ij} - W_{ij}/2, \alpha_{ij} + W_{ij}/2)\}|/N, \tag{2}$$

where α_{ij} and W_{ij} are the bisector azimuth and the width values of the i-th sector of the j-th explosion, and N is the total number of the explosions in the dataset. This calculation is done while not considering the axisymmetric part.

https://doi.org/10.5194/egusphere-2025-6539
Preprint. Discussion started: 12 January 2026

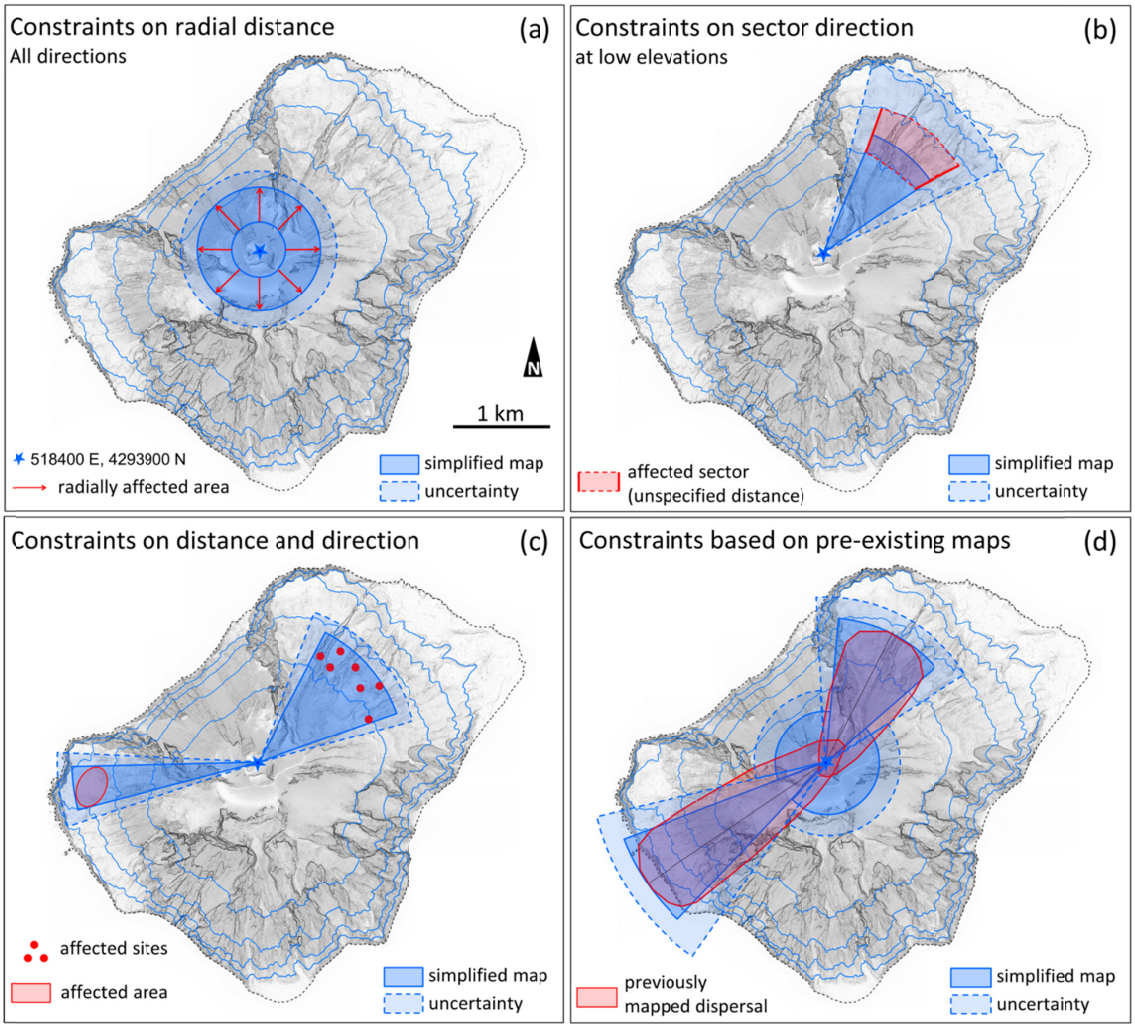

Figure 2: Examples of simplified mapping data on: (a) affected radius, (b) affected sectors at low elevation, (c) affected sites or areas, (d) pre-existing maps of ballistic dispersion. The red arrows, shapes, and dots indicate the spatial observation data processed. The solid blue circular sectors show the areas assumed as affected, and the dashed blue shapes are the areas uncertainly affected. A blue star marks the center of Crater Terrace.

https://doi.org/10.5194/egusphere-2025-6539
Preprint. Discussion started: 12 January 2026

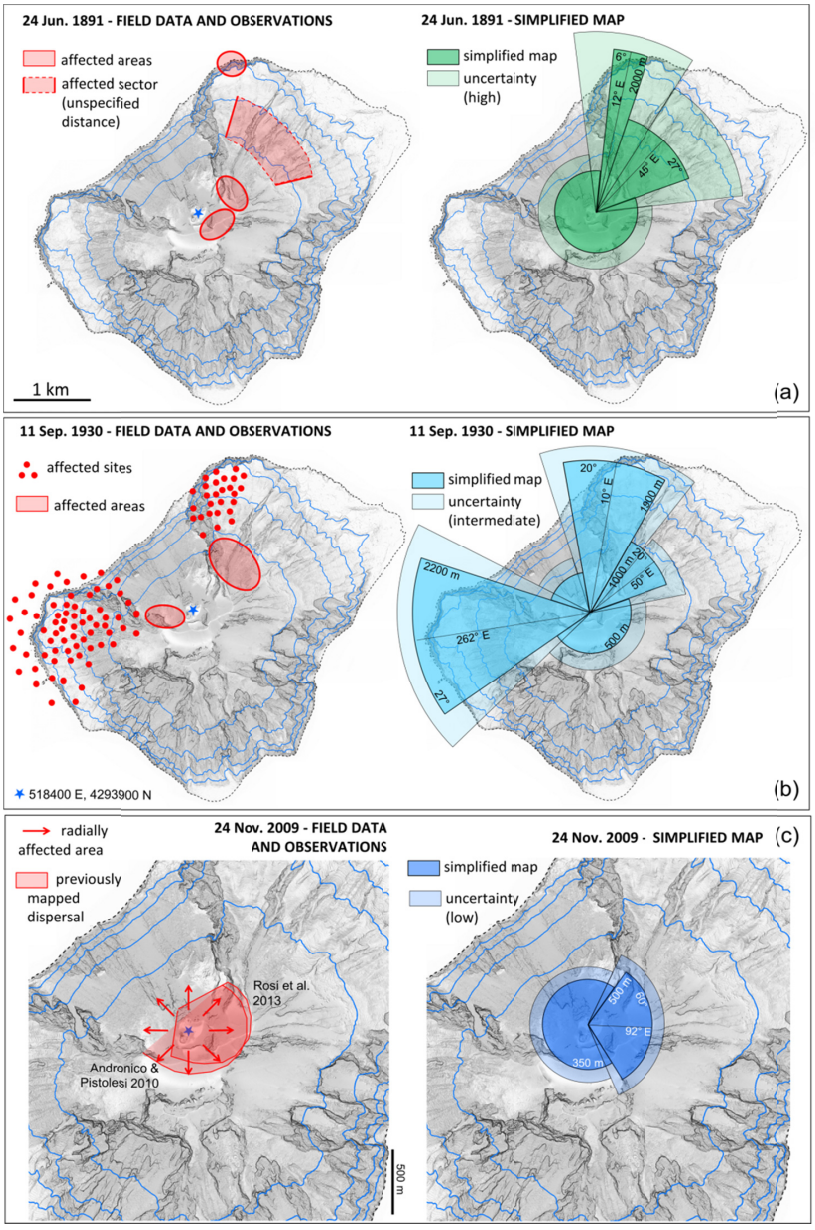

Figure 3: Three examples of field data (left) and resulting simplified maps (right) of the areas affected by ballistics, including measurements of maximum distances, directional angles, and sector widths. See also Supporting Text S1 and S2, Tables S1 and S2.
230 **Different hues indicate different uncertainty classes: blue for low, azure for intermediate, green for high uncertainty. The boundary areas in lighter colors around each sector represent the uncertainty considered.**

https://doi.org/10.5194/egusphere-2025-6539
Preprint. Discussion started: 12 January 2026

Table 1: Summary of the uncertainty classes associated with the ballistic maps.

Uncertainty class	Radial uncertainty	Angular uncertainty	Types of events
Low	Uniformly sampled between 0 and 100 m.	Uniformly sampled between 0 and 16 degrees.	Major explosions with available maps of ballistic fallout.
Intermediate	Uniformly sampled between0 and 200 m.	Uniformly samples between 0 and 32 degrees for major explosions, between 0 and 16 degrees for paroxysms.	Major explosions without available maps, paroxysms with mapped or detailed ballistic fallout in every direction.
High	Uniformly sampled between 0 and 200 m if sufficiently constrained, See in the notes if weakly constrained.	Uniformly sampled between 0 and 32 degrees.	Paroxysms with weak constraints to the ballistic fallout in some directions. The weakly constrained radii are uniformly sampled: a) between 1200 m and 1800 m if low elevation portions of the island are affected unspecifically, and (b) between 500 m to 1000 m if Sciara del Fuoco is widely affected by ballistic fall but without projectiles going directly offshore.

https://doi.org/10.5194/egusphere-2025-6539
Preprint. Discussion started: 12 January 2026

3 Data

In this study, we analyze two open INGV catalogs of major explosions and paroxysms at Stromboli, summarized in Figure 4. The first catalog (Bevilacqua et al., 2020a), named "historical catalog", is the review of more than a hundred scientific literature sources from 1879 to 1960. The ballistics of the major explosions listed in the historical catalog are not possible to map, only those of some of the historical paroxysms are mappable. No major explosion or paroxysm has been recorded between 1960 and 1970. The second catalog (Bevilacqua et al., 2023), named "recent catalog", is the detailed review of monitoring bulletins and reports, previous catalogs, and scientific literature of the last ca. 50 years, i.e. the period from 1970 to 2023 (more details in the Open Research Statement and in Supporting Texts S1 and S2). It should be noted that the catalogued record is possibly affected by under recording of major explosions occurred between 1960 and 1985, due to the cessation of military observations on Stromboli.

The historical catalog and a preliminary recent catalog up-to-date at 31/08/2020 were both statistically analyzed in terms of inter-event times, cluster analysis and annual rates in Bevilacqua et al., (2020b). The new version of the historical catalog analyzed here was released in January 2024 and includes a few additional events due to further bibliographic research, i.e., 4 paroxysms, 2 major explosions, 4 uncertain major explosions. Similarly, the recent catalog used here differs from the data analyzed in Bevilacqua et al. (2020b) in that the former includes ca. 3 years of new events and a more detailed description of the major explosions and of the uncertain major explosions, which was essential for mapping the ballistic projectiles distribution. In both INGV catalogs we acknowledge the incorporation of all the information contained in previous datasets of explosive activity at Stromboli, e.g., Barberi et al. (1993), Jaquet and Carniel (2003), Falsaperla and Spampinato (2003), Rosi et al. (2013), Calvari and Nunnari (2023), after the investigation of the original sources that first-hand described the phenomena, and that are summarized in Supporting Texts S1 and S2 for what concerns the ballistic fallout.

3.1 Analysis of maximum distance, direction and area affected by ballistic projectiles

The recent catalog encompasses 51 major explosions and 34 uncertain major explosions, i.e. explosions of unclear characterization that could have been major explosions or ordinary activity. We mapped the areas affected by ballistic fallout for the majority of explosions included in this recent catalog. In detail, we managed to map 43 events, i.e., ca. 85% out of the 51 major explosions.

The collection of 43 mapped major explosions is made of 37% low uncertainty maps, and 63% intermediate uncertainty maps, all reported in Figures 5 and 6. Of these maps, 5% include three sectors, 33% two sectors, 62% one sector. In just one event, i.e. 2008-B, the distribution is radial and we mapped it by one full circular sector with a radius equal to its axisymmetric part. In 23% of the mapped major explosions one of the sectors is directed towards Sciara del Fuoco, but in 56% the information about the ballistic distance in Sciara del Fuoco is unclear. Therefore, under-recording of ballistics projectiles in Sciara del Fuoco may be significant for major explosions.

https://doi.org/10.5194/egusphere-2025-6539
Preprint. Discussion started: 12 January 2026

3.2 Collection of simplified maps of ballistic projectile distribution of paroxysms

The historical catalog Bevilacqua et al. (2020a) describes 36 paroxysms and the recent catalog Bevilacqua et al. (2023) describes 4 paroxysms. We mapped 20 out of 36 historical events and all the recent events, i.e., ca. 60% of the paroxysms from 1879 to 2023. The collection of 24 mapped paroxysms encompasses 33% intermediate uncertainty maps and 67% high uncertainty maps, all reported in Figure 7. Of these maps, 21% include three sectors, 54% two sectors, and 25% one sector. In 54% of the mapped paroxysms one of the sectors is directed towards Sciara del Fuoco and in 24% the information on the ballistic distance in Sciara del Fuoco is not specifically quantified. The under-recording of ballistics ejected towards Sciara del Fuoco is therefore likely also for the paroxysms.

https://doi.org/10.5194/egusphere-2025-6539
Preprint. Discussion started: 12 January 2026

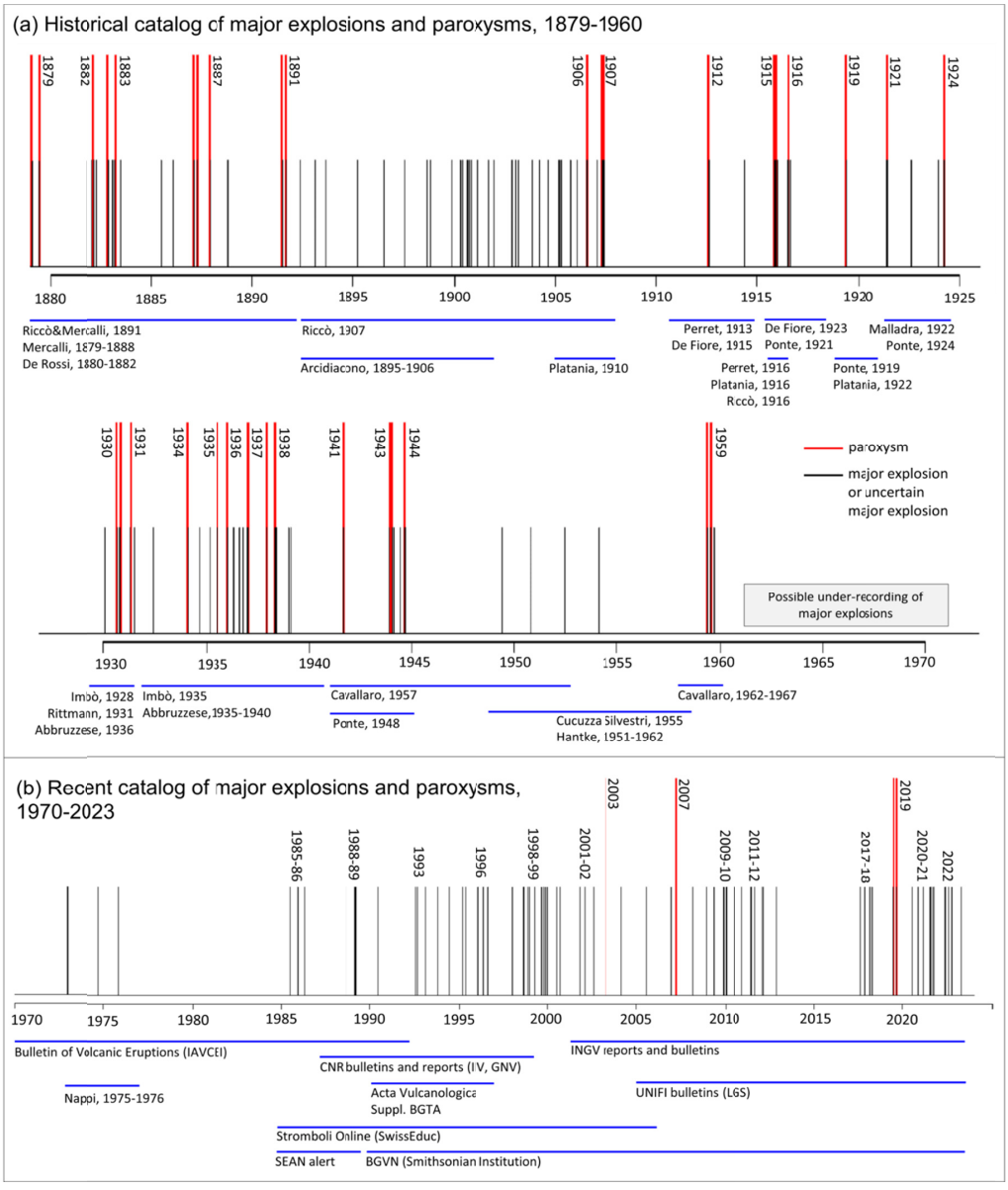

275 **Figure 4: (a) Historical catalog of major explosions and paroxysms at Stromboli from 1879 to 1960, (b) recent catalog from 1970 to 2023. Black bars mark the major explosions including the uncertain major explosions, and red bars mark the paroxysms. Below the bar plots, the time intervals described in the key literature sources labeled, fully listed in Supporting Texts S1 and S2, are reported. Figure S3 shows the catalogs without the uncertain major explosions; Table S3 lists the full explosion record of the two catalogs.**

https://doi.org/10.5194/egusphere-2025-6539
Preprint. Discussion started: 12 January 2026

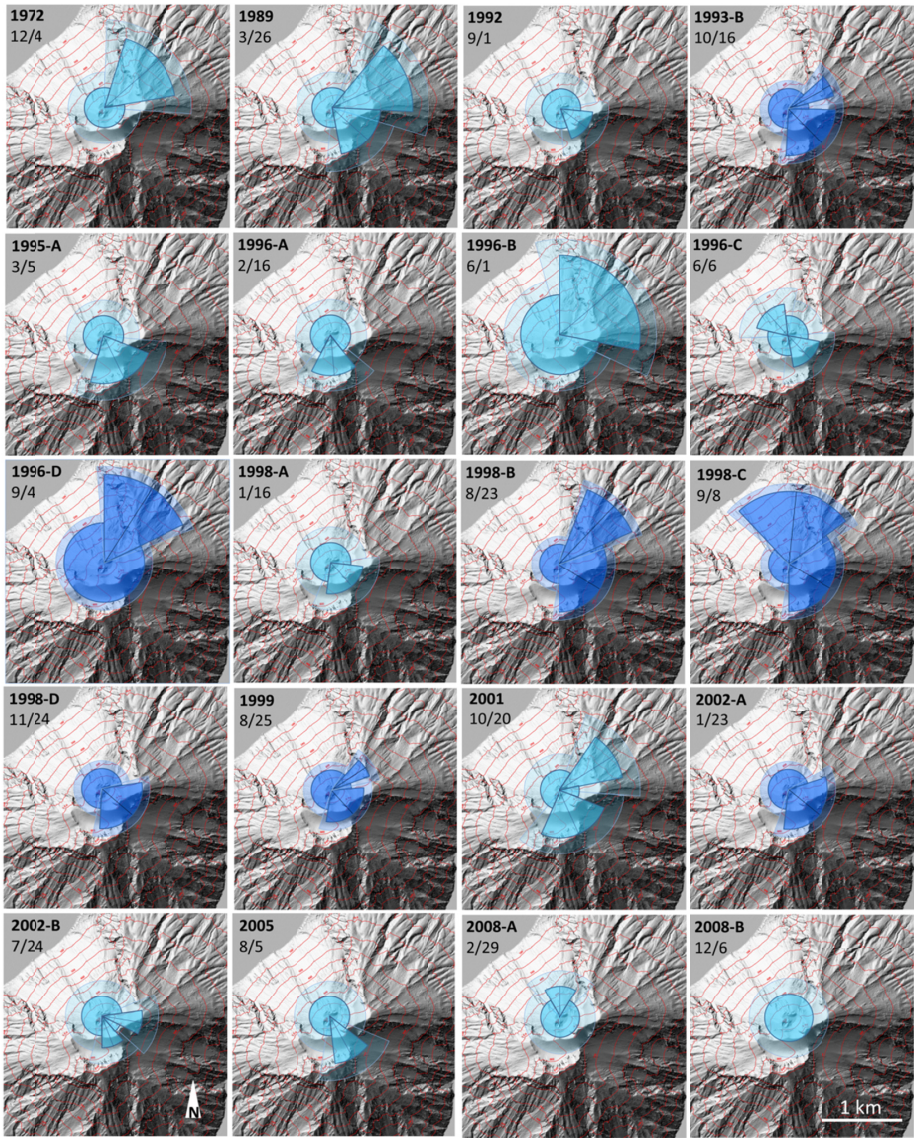

280

Figure 5: Simplified spatial maps of the areas affected by ballistic projectiles for 20 major explosions from 1970 to 2008. Different hues indicate different uncertainty classes: blue for low, azure for intermediate uncertainty. Lighter color areas mark the uncertainty considered. In Table S1 are reported the distances and angles of the sectors of all events considered and labeled as in the figure. Maps detailed in Supporting Text S1.

https://doi.org/10.5194/egusphere-2025-6539
Preprint. Discussion started: 12 January 2026

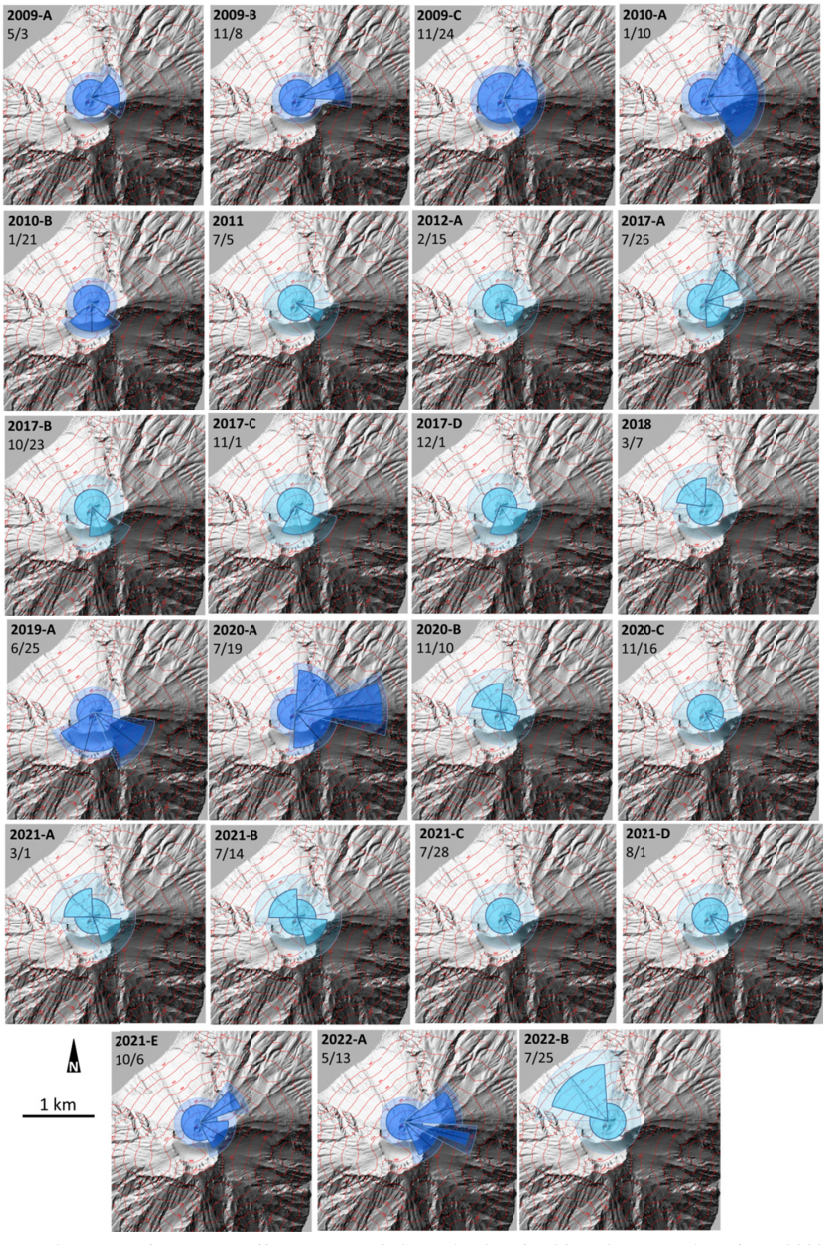

285

Figure 6: Simplified spatial maps of the areas affected by ballistic projectiles for 23 major explosions from 2009 to 2023. Different hues indicate different uncertainty classes: blue for low, azure for intermediate uncertainty. Lighter color areas mark the uncertainty considered. In Table S1 are reported the distances and angles of the sectors of all events considered and labeled as in the figure. Maps detailed in Supporting Text S1.

https://doi.org/10.5194/egusphere-2025-6539
Preprint. Discussion started: 12 January 2026

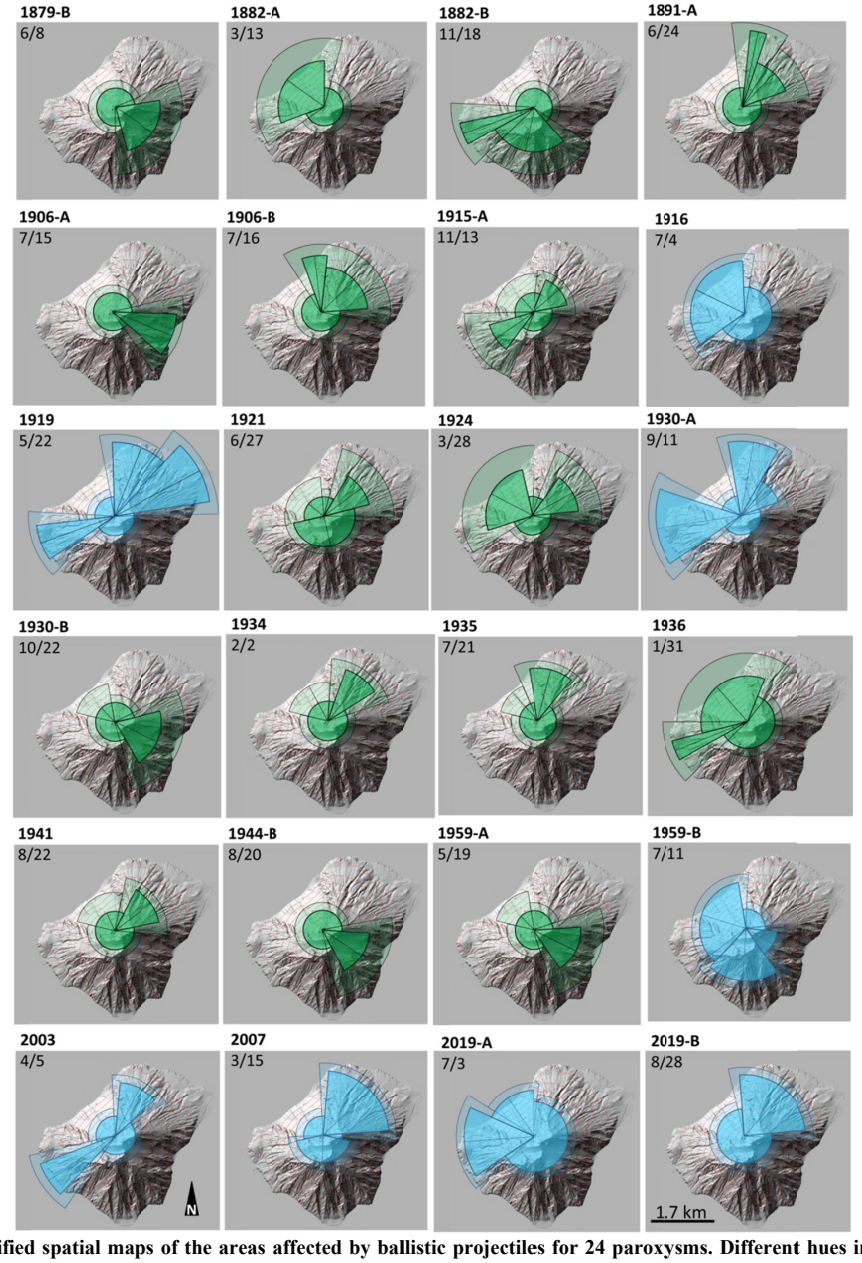

290 **Figure 7: Simplified spatial maps of the areas affected by ballistic projectiles for 24 paroxysms. Different hues indicate different uncertainty classes: azure for intermediate, green for high uncertainty. Lighter color areas mark the uncertainty considered. In Table S2 are reported the distances and angles of the sectors of all events considered and labeled as in the figure. Maps detailed in Supporting Text S2.**

https://doi.org/10.5194/egusphere-2025-6539
Preprint. Discussion started: 12 January 2026

4 Results

4.1 Statistical description of the distance of ballistic projectiles

Figure 8 describes the distribution of the maximum distances of ballistic projectiles from the center of the Crater Terrace in each specific event considered. In particular, Figures 8a and 8b list the maximum distances reached in major explosions and paroxysms, respectively, and indicate the 90% uncertainty intervals of the probability estimates. These data are plotted chronologically, while Figure S4 shows the same data plotted in ascending order.

The following percentage estimates are evaluated by counting the events in a Monte Carlo simulation that uniformly sampled the distance uncertainty. Figure 8c summarizes that in 23% to 37% of the major explosions the maximum distances were less than 500 m; in 51% to 65% they were above or equal to 500 m but less than 1000 m; in 12% to 14% above of 1000 m. Figure 8d summarizes that in 17% to 42% of the paroxysms the maximum distances were less than 1500 m; in 29% to 54% they were above or equal to 1500 m but less than 2000 m; in 25% above of 2000 m but less than 2500 m; in 4% above 2500 m. It should be noted that in both the collections of major explosions and paroxysms there is a greater uncertainty on the maximum distances of small-size events, than of the large-size events. Table S4 summarizes all the described values.

Finally, Figure 8e shows the combined exceedance probability functions obtained by sampling from the distances in Figures 8a and 8b, and by weighting the paroxysms 12% of the total, which is the event ratio recorded in Tables S1 and S2 from 2003 to 2023. It should be noted that the fraction of paroxysms with respect to the total of major explosions and paroxysms would decrease to 7.3% if evaluated between 1970 and 2023, because of the complete absence of paroxysms between 1959 and 2003 (Bevilacqua et al. 2020b). This plot represents the continuous distribution of maximum distances of the two phenomena.

Figure 9 considers the ballistic distances in all dispersal sectors chronologically, i.e., 61 sectors for the major explosions, in Figure 9a, and 47 sectors for the paroxysms, in Figure 9b. Figure S4 shows the same data plotted in ascending order. It should be noted that the same explosion possibly achieved different distances in each sector because of the asymmetrical features described in Texts S1 and S2, and therefore up to three values can correspond to the same explosive event. In this way, the distances are statistically lower than in Figure 8, and there are more distance values than the number of events, because the description of the ballistic projectiles distribution is not limited to the maximum distance. Moreover, this description equally counts all sectors, regardless of their width, and it does not consider the axisymmetric part of the explosions.

In Figures 9c and 9d, we plotted the exceedance probability functions obtained by sampling from the distances in Figures 9a and 9b after weighting the sectors according to their width. For the major explosions, we obtained a probability of 64% ±6.5% to exceed 500 m, of 18% ±4.5% to exceed 750 m, and of 8% ±1.5% to exceed 1000 m. For the paroxysms, we obtained a probability of 79% ±2.0% to exceed 1000 m, of 48% ±11% to exceed 1500 m, of 13% ±2.0% to exceed 2000 m,

https://doi.org/10.5194/egusphere-2025-6539
Preprint. Discussion started: 12 January 2026

of 1.5% ±0.5 to exceed 2500 m. All these estimates do not consider the proximal axisymmetric part; if we include it, thus fully representing the distribution of mapped ballistic distances in all directions, this produces probabilities of exceedance up to ca. 3 times lower, and reported in Table S4. Figure S5 shows the exceedance probability only of the maximum distance, and only of the proximal axisymmetric part.

4.2 Statistical description of the direction of ballistic projectiles

Figure 10 shows the range graphs and probability percentage of ballistic sectors directions. This was done while not considering the proximal axisymmetric part, because otherwise the statistics would have covered a round angle for every explosion. Figure 10a details the range graphs of the 61 sectors of 43 mapped major explosions from 1970 to 2023. In this case, 57% of the circular sectors have bisectors in the SE quadrant, 30% in the NE quadrant, 10% in the NW quadrant, 1.5% in the SW quadrant and 1.5% have no preferential direction. Table S4 summarizes all the described values. We note that the paroxysms in 2003 and 2007 were followed by a general shift towards N in the directions of the next major explosions; this did not happen after the paroxysms occurred in 2019. Similarly, Figure 10b details the range graphs of the 47 sectors of 24 mapped paroxysms from 1879 to 2023. In this case, 34% of the bisectors fell in the NE quadrant, 30% in the NW, 21% in the SW and 15% in the SE quadrant.

In Figures 10c and 10d we plotted the probability percentage of the ballistics directions, as a function of the azimuth angle. Figure 10c shows the probability percentage of the ballistics directions for major explosions. The function has a maximum of 77% ±2% at 140°E ±10°, i.e., in the SE direction, and a minimum of 0% at 250°E ±10°, i.e., in the SW direction. This latter value may be affected by some under-recording of major explosions in the SW direction. The angular uncertainty in these estimates is equivalent to the width of the maximum values in the 95th percentile plot. Figure 10d shows the probability percentage of the ballistics directions for paroxysms. The function has a maximum of 70% ±9% at 355°E ±10°, i.e., in the N direction, and a minimum of 19% ±2% at 175°E ±10°, i.e., in the S direction. In addition, a plateau above 50% is observed from NE to W clockwise. It should be noted that major explosions and paroxysms are dispersed in significantly different directions, due to the complex interplay of conduit+craters' architecture, and the different scales of these events, in terms of magma volume and energy. Figure S6 shows the results only considering the sectors of maximum distance. See Table S4 for more details.

4.3 Statistical description of the total area of ballistic projectiles distribution

Figure 11 shows the histograms of the width of the circular sectors and of the total area affected by projectile fallout. Figures 11a and 11b do not consider the proximal axisymmetric part, and just focus on the circular sectors. In particular, Figure 11a is the histogram of the width of the 61 sectors of 43 mapped major explosions from 1970 to 2023. The mean width value is 90°, with 5th percentile of 41° and 95th percentile of 136°. Similarly, Figure 11b is the histogram of the width of the 47 sectors of 24 mapped paroxysms from 1879 to 2023. In this case the mean width value is again 90°, with 5th percentile of 33°

https://doi.org/10.5194/egusphere-2025-6539
Preprint. Discussion started: 12 January 2026

and 95th percentile of 183°. In fact, the sectors of the paroxysms have a similar average width to the sectors of the major explosions, but sectors wider than 150° are only observed for the paroxysms. Figure S3 shows the histogram of the width only of the sectors of maximum distance.

Figures 11c and 11d are the histograms of the total area affected by ballistics of major explosions and paroxysms, respectively. The mean area value of major explosions is 6.9 × 10^4 m^2, with the 5th percentile of 3.3 × 10^4 m^2 and the 95th percentile of 14.8 × 10^4 m^2. The mean area of paroxysms is 3.6 × 10^5 m^2, with the 5th percentile of 2.0 × 10^5 m^2 and 95th percentile of 6.1 × 10^5 m^2. These values are 4 to 6 times larger than those of major explosions. The histogram of major explosions total area is characterized by a relatively longer tail than the histogram of paroxysms, and this tail is partially overlapping with their values. In fact, in the former case the maximum value is ca. +70% of the 95th percentile, while in the latter is ca. +20%. Table S4 summarizes all the statistics in this paragraph. Finally, Figure 11e shows the combination of the histograms in Figure 11c and 11d, by weighting the paroxysms 12% of the total, similarly to Figure 8e. Also in this case, the distribution of the areas is continuous between major explosions and paroxysms: the former representing the bulk and the latter the tail.

https://doi.org/10.5194/egusphere-2025-6539
Preprint. Discussion started: 12 January 2026

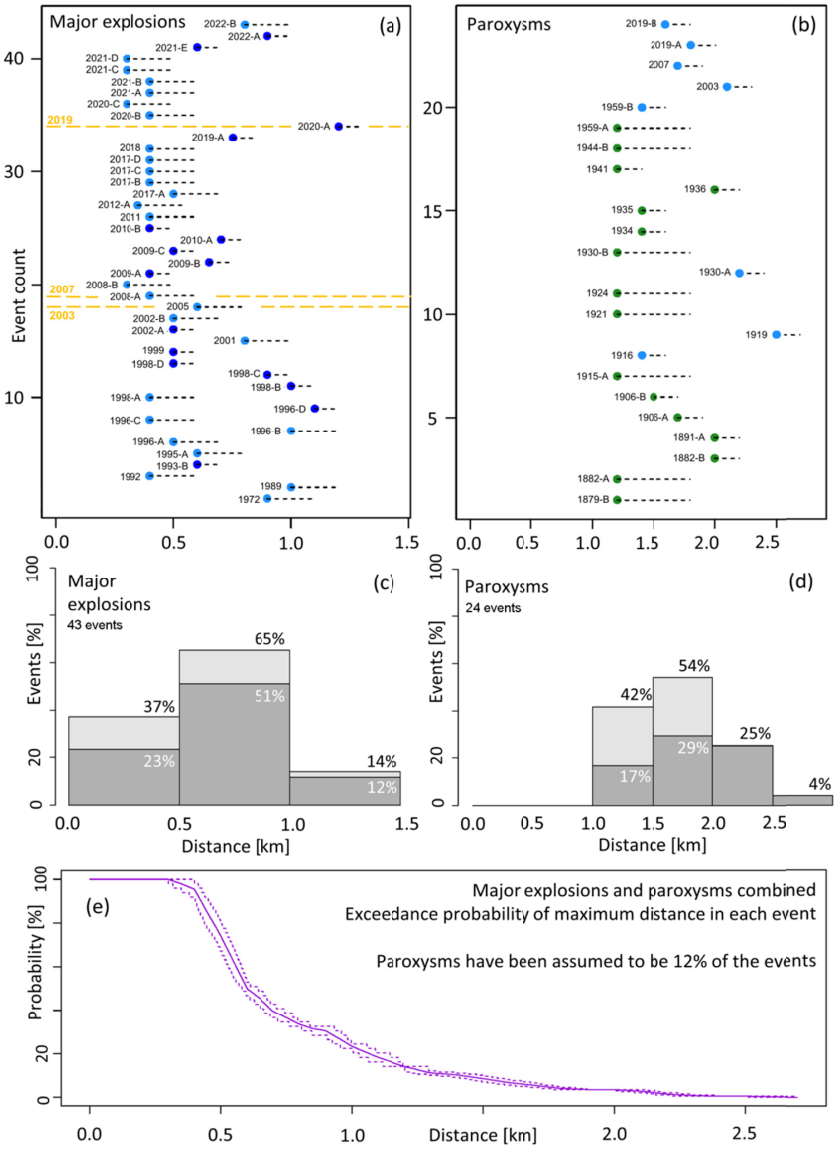

Figure 8: List of the maximum ballistic distances in each event, in (a,b) arranged in chronological order from bottom to top of each panel, in (c,d) partitioned in distance bins, in (e) the exceedance probability function. In (a,c) we show the major explosions and in (b,d) the paroxysms, in (e) combined together. In (a) the paroxysms are marked by orange dashed lines. In (a,b) the colors distinguish the classes of uncertainty, i.e. blue is low, azure is intermediate, green is high. The dashed lines highlight the uncertainty considered: the colored dots indicate the recorded values and the dashed line their possible increase. The light colored bars in (c,d) and the dashed lines in (e) are the 5th and 95th percentiles of uncertainty. In (e) the paroxysms have been assumed to be the 12% of all events as results from the analysis of the last two decades (2003-2023).

https://doi.org/10.5194/egusphere-2025-6539
Preprint. Discussion started: 12 January 2026

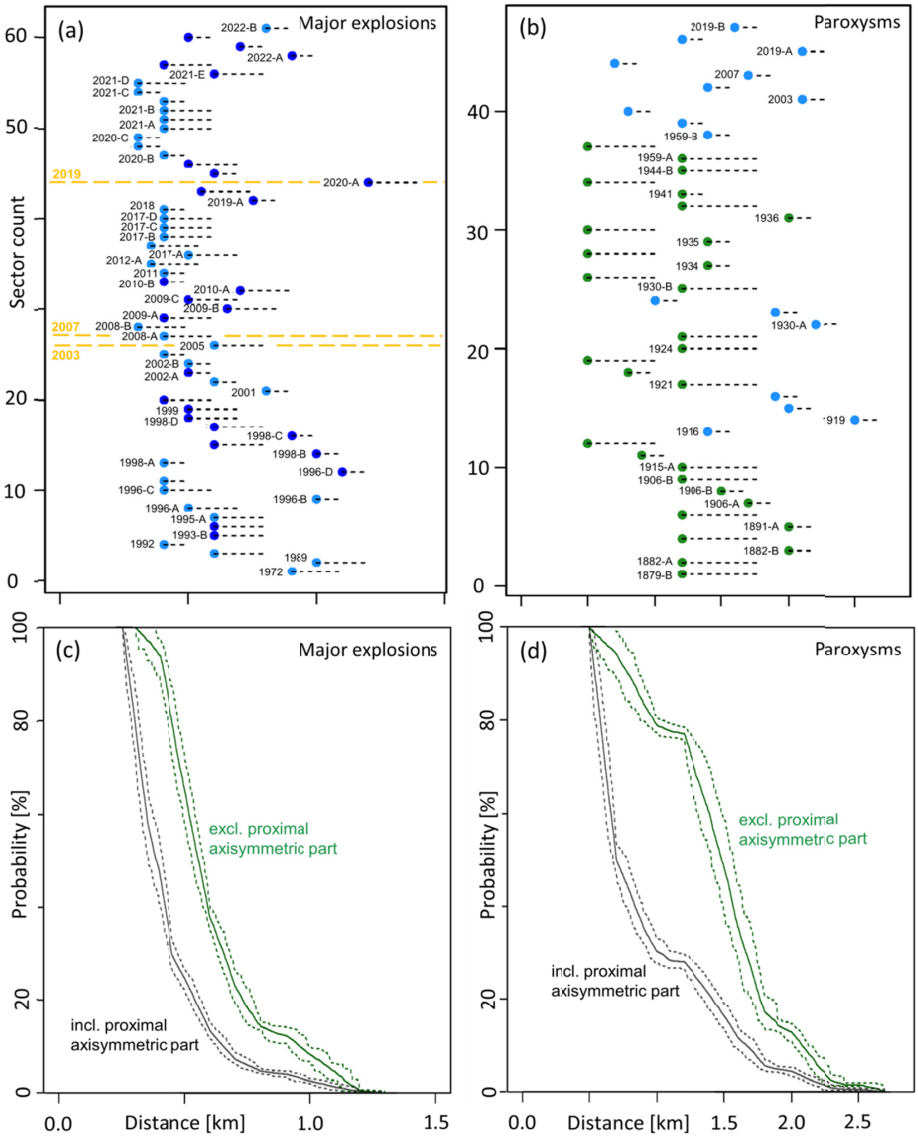

380 **Figure 9: (a,b) List of the ballistic distances, arranged in chronological order from bottom to top of each panel, by considering all the circular sectors involved. For each explosion it is labeled only the sector in which the largest distance was achieved. The colors distinguish the classes of uncertainty. (c,d) Exceedance probability function of the ballistic distances in all sectors, in green by excluding the proximal axisymmetric part, in black by including it. The circular sectors are weighted according to their width. In (a,c) we show the major explosions and in (b,d) the paroxysms; in (a) the paroxysms are marked by orange dashed lines. In (a,b)**
385 **the dashed lines highlight the uncertainty considered: the colored dots indicate the recorded values and the dashed line their possible increase. In (c,d) the dashed lines represent the 5th and 95th percentiles of uncertainty.**

https://doi.org/10.5194/egusphere-2025-6539
Preprint. Discussion started: 12 January 2026

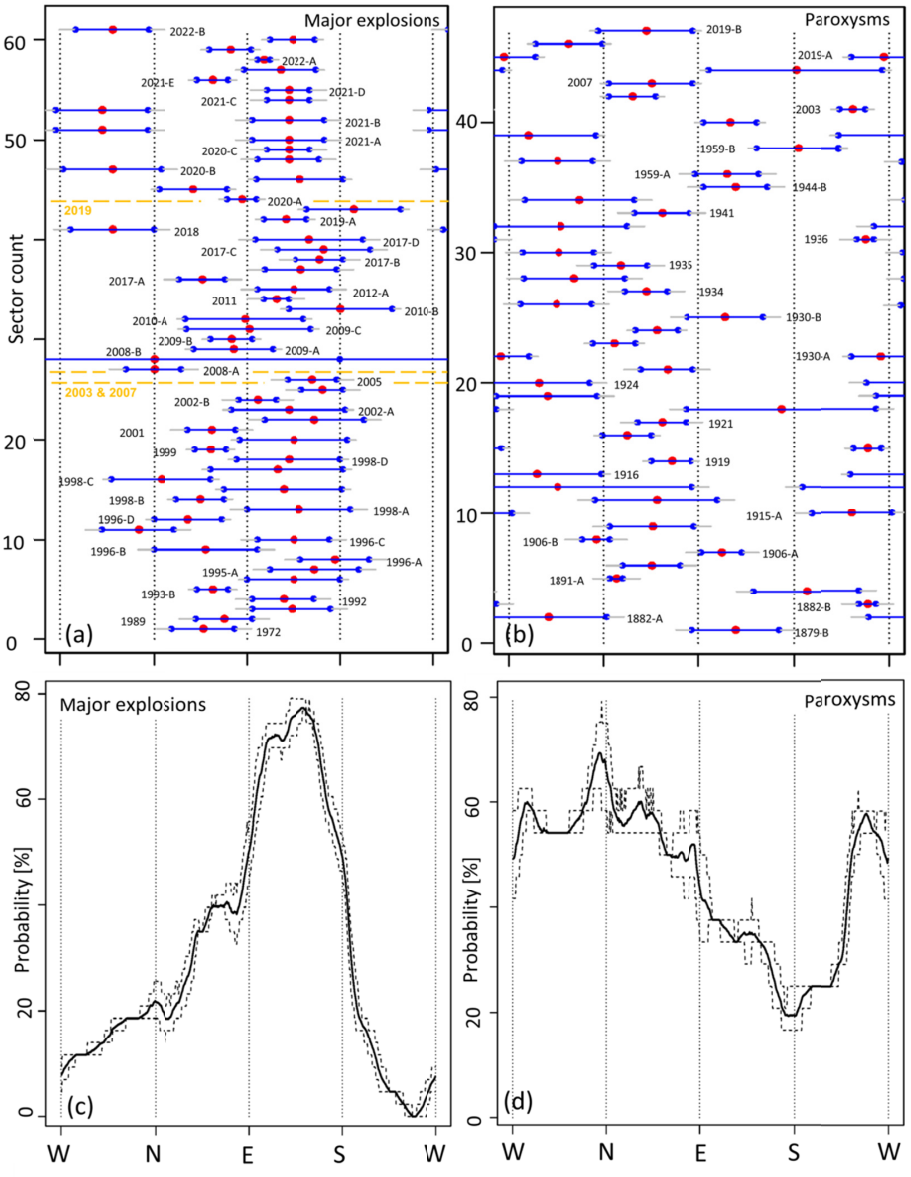

Figure 10: (a,b) Range graphs of the ballistic sectors direction (red dots) and width (blue lines). All directional sectors of each paroxysm are considered, and for each explosion it is labeled only the sector in which the largest distance was achieved. The 390 **counting index is ordered chronologically among different events, from the bottom to the top of each plot. The uncertainty is represented in gray. In (a) the paroxysms are marked by orange dashed lines. (c,d) Ballistics direction probability percentage. The dashed lines are 5th and 95th percentiles of the associated uncertainty. In (a,c) we show the major explosions and in (b,d) the paroxysms.**

https://doi.org/10.5194/egusphere-2025-6539
Preprint. Discussion started: 12 January 2026

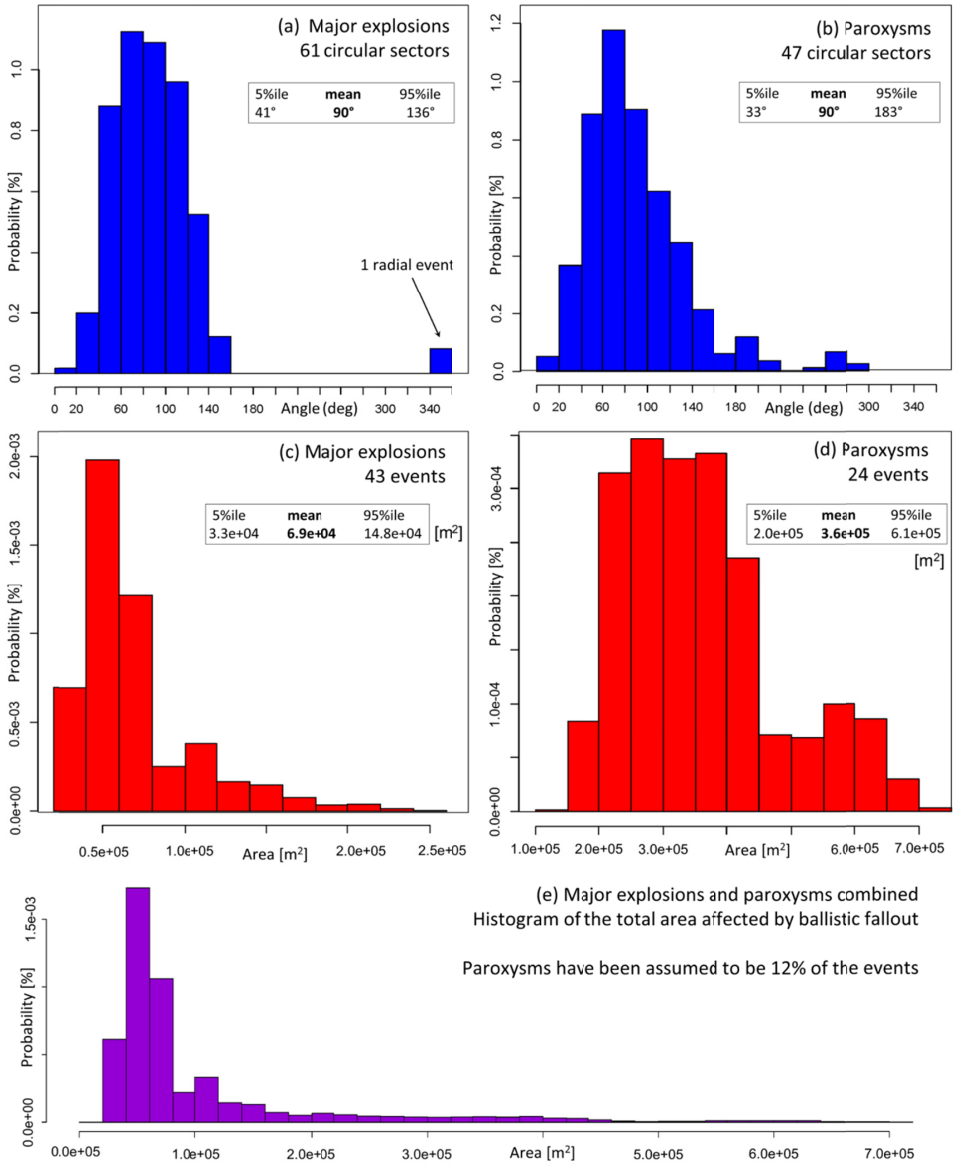

395 **Figure 11: Histograms of (a,b) the width of all the circular sectors not considering the axisymmetric part, and of (c-e) the total area affected by projectile fallout. In (a, c) are mapped the major explosions, in (b, d) the paroxysms, in (e) combined together. In (e) the paroxysms have been assumed to be the 12% of all events as results from the analysis of the last two decades (2003-2023). The sample count includes a Monte Carlo simulation of the random effects of mapping uncertainty, i.e., 10^3 replicas for every sector in (a,b), 10^2 replicas for every event in (c,d).**

400

https://doi.org/10.5194/egusphere-2025-6539
Preprint. Discussion started: 12 January 2026

5 Discussion

A first novel contribution of this study is the investigation effort to reconstruct and map a significant number of areas affected by ballistic fallout generated by major explosions and paroxysms at Stromboli. It should be noted that only a small fraction, i.e., ca. 1/4, of major explosions and paroxysms were previously mapped. This study aimed at filling such knowledge gap and collected all available information on past ballistic fallout at Stromboli, rich but sparse into tens of articles many of which were written at the end of the XIX Century and in the first half of the XX Century, mostly in Italian or in German.

A major difficulty related to this investigation was that the Island of Stromboli is characterized by a complex history of place names (i.e., toponyms), and their evolution has been a matter of semantic and ethnographic research, since the XIX century (Asburgo, 1896; Losacco, 1973; Texts S1 and S2). For this reason, the full understanding and geographical interpretation of the documents describing past ballistic fallouts was often a complex duty, significantly intertwined with uncertainty quantification guided by expert judgment. This was achieved by the authors' group without following a formal procedure to quantify their judgement but simply through discussion and reaching a group consensus.

Moreover, our study required a changed approach with respect to the classical problem of reconstructing the detailed footprint of ballistic dispersion of a single explosive event, up to the geographic coordinates of the single greatest clasts (e.g., Bertagnini et al., 1999; Andronico and Pistolesi, 2010; Pistolesi et al., 2008; 2011). Our new method to map the areas of ballistic fallout was based on the representation of the area affected through a circular proximal area and up to three circular sectors of variable radius and width. Such a statistical approach has the advantage of representing each explosion in terms of a minimum number of scalar parameters: 1 to 4 distances and up to 6 angles. Moreover, every scalar estimate was naturally related to an uncertainty range, which was an output of our investigation. In addition, these uncertainties enabled us to neglect the variability and multiplicity of explosion sources, and the detailed shape of the directional lobes of ballistic fallout, while tailoring the maps of past events. Without following this simplified approach, it would have been impossible to map most of past events, and, ultimately, to collect a sufficient dataset of ballistic fallouts to be used to produce probabilistic hazard assessment maps at Stromboli (see companion manuscript Bevilacqua et al., submitted).

A second novel contribution of our investigation was the quantitative characterization of the areas affected by ballistic fallout generated by major explosions and paroxysms at Stromboli as represented by the simplified maps produced. The distinction between these two categories is the traditional way in which the volcanological community described the explosions more intense than the ordinary activity at Stromboli. This terminology is rooted in the XIX Century language (e.g., Mercalli, 1883; Riccò 1907; Ponte, 1916; Imbò, 1928), but it was formalized with its modern meaning only from the last decade of XX Century (e.g., Barberi et al., 1993; Rosi et al., 2013; Bevilacqua et al., 2020b).

We showed that major explosions and paroxysms primarily differ in their maximum and mean ballistic distances, which are roughly twice for the paroxysms. However, these two categories are adjacent, and partially overlapping, in terms of their

https://doi.org/10.5194/egusphere-2025-6539
Preprint. Discussion started: 12 January 2026

ballistic ranges (see Fig. 8). In particular, the greatest distance of every major explosion in our dataset, i.e. 1200 m plus uncertainty, was observed in the event of 19th July 2020. In fact, based on ground deformation data that event was placed at the boundary between major explosions and paroxysms by Voloschina et al. (2023), and it was considered a paroxysmal explosion according to the classification method proposed by Calvari et al. (2021). The greatest distance of every paroxysm in our dataset, i.e. 2500 m plus uncertainty, was observed in the event of 22nd May 1919, which produced significant ballistic damage to the buildings in the Stromboli village (Ponte et al., 1919; 1924; Ranfaldi, 1921; Platania et al., 1922).

A comprehensive probability distribution of maximum ballistic distances at Stromboli should merge the major explosions and the paroxysms, but the estimate of their occurrence ratio is difficult to compute. In fact, major explosions before 1970 are affected by significant uncertainty and likely under-recording issues. Moreover, only 5 paroxysms occurred after 1970, and their time series is irregular and characterized by temporal clusters and a 44-year gap between 1959 and 2003 (Bevilacqua et al., 2020b). As a consequence the fraction of the number of paroxysms over the number of all explosions (i.e., major explosions plus paroxysms) was 12% from 2003 and 2023, but dropped down to 7.3% from 1970 to 2023. Conversely, the same ratio grew to ca. 19% if we considered all the paroxysms and the major explosions from 1879 to 2023, even after we included all the uncertain major explosions (see Table S3). Therefore, we assumed 12% as a plausible and relatively robust estimate of this important scale parameter.

In addition to their distinct ballistic distances, we showed that major explosions and paroxysms also differ in terms of their asymmetric directions of furthermost ballistic dispersal. In fact, while the major explosions have a peak probability towards SE, the paroxysms have two peaks towards N and WSW (more details in Figure 10). It should be noted that the most frequented trails, from N to SE, and inhabited areas, towards NE and WSW, are the easiest places to survey in the hours/days after the explosions, and their directions roughly include those of peak probabilities. For this reason, in the production of ballistic hazard maps based on past data it is very important to develop *ad hoc* methods to mitigate potential under recording biases (see companion manuscript Bevilacqua et al., submitted).

As a matter of fact, the areas affected by ballistic fallout of past explosions are essentially characterized by past data, and they clearly are not axisymmetric. Physical reasons for these asymmetries should be investigated case by case. In general, the paroxysms appear able to re-shape the shallow conduits and craters more greatly and deeply than major explosions (Rittmann, 1931; 1933; Civico et al., 2021; 2024; Zuccarello et al., 2025), and this might significantly affect the trajectories of ballistics (e.g., Valentine et al. 2012; Taddeucci et al. 2013). It should be noted that within the large paroxysms of Stromboli described in Bertagnini et al. (2011), which occurred in 1930 and in the 16th Century, a different nature of lithic clasts suggested the involvement of different portions of the upper conduit during the crater excavation.

With this respect, experimental studies on the craters obtained by several detonations showed that the depth of the explosion and of a pre-existing crater morphology can have a distinctive effect on the evolution of the craters and the consequent jet and dispersal of ballistic projectiles (Valentine et al., 2014; Graettinger et al., 2014). Furthermore, it was observed that

https://doi.org/10.5194/egusphere-2025-6539
Preprint. Discussion started: 12 January 2026

experimental craters created by several detonations in layered aggregates, as in the case of Stromboli, can significantly differ from a single-blast (Sonder et al., 2015). These differences may be even more evident in the case of short-lived explosions such as major explosions and paroxysms occurring from sub-vertical or inclined shallow conduits, because the conduit and crater walls formed by each event are likely different from those existing before the same event (Valentine et al. 2015; Schmid et al., 2021; Sonder et al., 2022; Civico et al., 2021; 2024).

In summary, there are clear evidences that the architecture and geometry of vents and shallow conduits greatly influence the ballistic dispersion: conduit and crater walls, layers, ridges and cones can all produce shielding effects, so enabling the generation of inclined jets, or be partially or entirely demolished into additional projectile fragments, depending on the explosion intensity, duration, and depth. All these complexities make the definition of input conditions for the numerical simulation of major explosions and paroxysms significantly uncertain when treated case-by-case, and very difficult to predict in general.

7 Conclusions

In this study, we presented a new method to map the ballistic fallout and quantified the key variables describing the areas affected by ballistic projectiles generated by several tens of past major explosions and paroxysms at Stromboli. The application of the new mapping method has allowed to build a new dataset of the areas affected by ballistics, complementary to the historical and recent catalogs of explosive activity of Stromboli. The new dataset, coming from all available scientific literature as well as monitoring and field/observation reports, allowed us to quantify the distances, directions and areas affected describing the ballistic fallout of major explosions and paroxysms, but also to estimate the size of the associated uncertainties. In the companion study, we will show how these data and analyses allow producing first probabilistic hazard maps of the areas affected by ballistic fallout with uncertainty quantification (Bevilacqua et al., submitted).

Based on the data and analyses presented these are the main outcomes and conclusions of the study:

1. A new dataset of the reconstructed areas affected by ballistic fallout from a total of 67 major explosions and paroxysms at Stromboli was produced based on a new simplified mapping method. Although the information has been collected over a significantly long period, i.e. ca. 150 years, and with details and accuracy quite different among them, the dataset represents, to our knowledge, a first attempt to systematically describe the areas potentially affected by ballistics and a key source of information for the quantification of the ballistic hazard at this volcano.

2. The dataset allowed analyzing the distribution of the maximum ballistic distances produced by major explosions and paroxysms from the center of Crater Terrace. A significant percentage of major explosions, i.e., from 23% to 37%, did not surpass 500 m ballistic distance; similarly, from 17% to 42% of the paroxysms did not reach 1,500 m ballistic distance. Nevertheless, in 12% to 14% of major explosions the ballistics reached 1,000 m distance, and 29% of the paroxysms reached 2,000 m. The combined distance distribution of major explosions and paroxysms

https://doi.org/10.5194/egusphere-2025-6539
Preprint. Discussion started: 12 January 2026

resulted to be remarkably continuous suggesting the absence of a net separation between the two categories in terms of generating mechanisms.

3. With the aim to produce probabilistic hazard maps, the statistics of the ballistic distance in all the circular sectors mapped in the past events analyzed was also computed, by weighting the sectors according to their width. Estimates were obtained by including the proximal axisymmetric part of explosions too. These two estimates are systematically lower than the maximum distance values discussed in point 2 above and will be both used in the companion study (Bevilacqua et al. submitted) to produce the hazard probability maps of ballistic fallout.

4. The directionality of the ballistic dispersal is remarkably asymmetric and differs significantly between major explosions and paroxysms. About 87% of the bisectors of major explosions fell towards the East half-plane, whereas 64% of the bisectors of the paroxysms fell towards the North half-plane. It was also possible to calculate the probability function of the ballistics directions, which for major explosions has a well-pronounced maximum of 77% ±2% at 140°E ±10° (i.e. towards SE) whereas for the paroxysms has a less evident maximum of 70% ±9% at 355°E ±10° (i.e. towards N).

5. For both the major explosions and the paroxysms, the mean width value of the circular sectors reconstructed was about 90°, but the paroxysms showed a greater variability in the 95th percentile values (up to about 180° with respect to about 130° for major explosions). The mean area of major explosions was 6.9×10^4 m^2, and the mean area of paroxysms was 3.6×10^5 m^2, i.e., ca. 5 times larger. However, the distribution of the areas affected is continuous between major explosions and paroxysms. As the ballistic distance, also the mean sector width and the area affected suggest the continuity between the two categories in terms of dispersal of ballistic particles.

6. The compiled map dataset accounts for the quantification of the uncertainties on the areas affected by the ballistic fallout of past events. This is a key feature of the dataset given the significant variability in the accuracy of the data and observations used. These sources of uncertainty were fully integrated in the statistical analyses, all conducted using Monte Carlo simulations that randomly perturb the data, and therefore reflected in the results presented. It is worth underlining that the results obtained were significantly robust with a limited influence of the uncertainties considered.

Finally, the study illustrates the fundamental importance of a continuous and detailed observation of the explosive activity of Stromboli for a quantitative description of its dynamics and a robust assessment of its hazards.

https://doi.org/10.5194/egusphere-2025-6539
Preprint. Discussion started: 12 January 2026

Data availability

The main historical sources that we relied upon are detailed in Supporting Text S1 and S2. In addition to the scientific publications, we considered several hundreds of monitoring and surveillance bulletins and reports regarding Stromboli volcano, issued by the "International Association of Volcanology and Geochemistry of the Earth Interior" (IAVCEI); by "Istituto Internazionale di Vulcanologia" (IIV) and "Gruppo Nazionale di Vulcanologia" (GNV) of "Consiglio Nazionale delle Ricerche" (CNR), by "Istituto Nazionale di Geofisica e Vulcanologia" (INGV), and by "Laboratorio di Geofisica Sperimentale" of Università di Firenze (UNIFI-LGS). We also considered the open documents on the "Stromboli Online" website by SwissEduc, the "Scientific Event Alert Network" (SEAN) and the "Global Volcanism Network" (GVN) of the Smithsonian Institution.

The historical catalog of major explosions and paroxysms at Stromboli (Bevilacqua et al., 2023), and the recent catalog of major explosions and paroxysms at Stromboli from 1970 to 2023 (Bevilacqua et al., 2020a) are available on the INGV - Sezione di Pisa. The derived data and the R scripts utilized for statistical analysis are available upon request.

Author contributions

All authors gathered, cured, and discussed the historical data, their classification, and uncertainty quantification of the past ballistic dispersions. A.B., P.L., P.D.C. drew the simplified maps. A.B. and A.N. conceived the main modeling ideas and scientific objectives. A.B. implemented the codes, performed the statistical analysis, and produced the graphs and plots. A.B. and A.N. prepared the first draft of the manuscript. All authors discussed the results, commented on the manuscript, provided critical feedback, and gave final approval for publication.

Competing interests

The contact author has declared that none of the authors has any competing interests.

Acknowledgements

This research has been supported by the INGV project "Rete Multiparametrica – Vulcani" and by "Piano di Potenziamento Stromboli EW-DPC, ex OCDPC n. 762/2021" and "Convenzione Attuativa per il potenziamento delle attività di servizio", Task 4.1, in the framework of "Accordo Quadro DPC-INGV 2022-2025". The contribution and support of ideas of many colleagues participating to the above projects are acknowledged. The manuscript does not necessarily represent official views and policies of the Dipartimento della Protezione Civile (Italy).

https://doi.org/10.5194/egusphere-2025-6539
Preprint. Discussion started: 12 January 2026

References

Alatorre-Ibargüengoitia, M. A., Delgado-Granados, H., Farraz-Montes, I. A. (2006), Hazard zoning for ballistic impact during volcanic explosionsat Volcán de Fuego de Colima (México). *Geological Society of America*, *Special Paper,* 402.

Alatorre-Ibargüengoitia, M. A., Delgado-Granados, H., Dingwell, D. B. (2012), Hazard map for volcanic ballisticimpacts at Popocatépetl volcano (Mexico). *Bull Volcanol* (9):2155–2169

Alatorre-Ibargüengoitia, M. A., Morales-Iglesias, H., Ramos-Hernández, S. G., Jon-Selvas, J., Jiménez-Aguilar, J. M. (2016), Hazard zoning for volcanic ballistic impacts at El Chichón Volcano (Mexico). *Nat Hazards* 81, doi: 10.1007/s11069-016-2152-0.

Andronico, D., and Pistolesi, M. (2010). The November 2009 paroxysmal explosions at Stromboli. *J Volcanol Geoth Res* 196, 120-125, doi: 10.1016/j.jvolgeores.2010.06.005.

Andronico, D., Del Bello, E., D'Oriano, C., Landi, P., Pardini, F., Scarlato, P., de' Michieli Vitturi, M., Taddeucci, J., Cristaldi, A., Ciancitto, F., Pennacchia, F., Ricci, T., and Valentini, F. (2021). Uncovering the eruptive patterns of the 2019 double paroxysm eruption crisis of Stromboli volcano. *Nat Comm* 12(1), 4213, doi: 10.1038/s41467-021-24420-1.

Aravena, A., Bevilacqua, A., de' Michieli Vitturi, M., Esposti Ongaro, T., Neri. A., Cioni, R. (2022). Calibration strategies of PDC kinetic energy models and their application to the construction of hazard maps. *Bull Volcanol* 84, 29, doi: 10.1007/s00445-022-01538-8.

Aravena, A., Bevilacqua, A., Neri, A., Gabellini, P., Ferrés, D., Escobar, D., Aiuppa, A., Cioni, R. Scenario-based probabilistic hazard assessment for explosive events at the San Salvador volcanic complex, El Salvador, *J Volcanol Geoth Res* 438, 107809.

Barberi, F., Rosi, M., Sodi, A. (1993), Volcanic hazard assessment at Stromboli based on review of historical data, *ActaVulcanol*, 3, 173–187.

Bebbington, M. S. (2013). Assessing spatio-temporal eruption forecast in a monogenetic volcanic field. *J Volcanol Geoth Res* 252, 14–28.

Bernard, B. (2018), Rapid hazard assessment of volcanic ballistic projectiles using long-exposure photographs: insights from the 2010 eruptions at Tungurahua volcano, Ecuador. *Volcanica*, 1(1): 49 – 61. doi: 10.30909/vol.01.01.4961.

Bertagnini, A., Coltelli, M., Landi, P., Pompilio, M., and Rosi, M. (1999). Violent explosions yield new insights into dynamics of Stromboli volcano. *Eos, Trans Am Geophys Union* 80(52), 633-636, doi: 10.1029/99EO00415.

Bertagnini, A., Metrich, N., Francalanci, L., Landi, P., Tommasini, S., Conticelli, S. (2008), Volcanology and magma geochemistry of the present-day activity: constraints on the feeding system. In: Calvari S, Inguaggiato S, Puglisi G, Ripepe M, Rosi M (eds) Learning from Stromboli. American Geophysical Union, *Geophys Mono* 182, Washington, DC, pp 19–38.

Bertagnini, A., Di Roberto, A., Pompilio, M. (2011), Paroxysmal activity at Stromboli: lessons from the past. *Bull Volcanol* 73, doi:10.1007/s00445-011-0470-3.

Bertin, D. (2017), 3-D ballistic transport of ellipsoidal volcanic projectiles considering horizontal wind field and variable shape-dependent drag coefficients, *J Geophys Res - Solid Earth* 122, 1126–1151, doi:10.1002/2016JB013320.

https://doi.org/10.5194/egusphere-2025-6539
Preprint. Discussion started: 12 January 2026

Bevilacqua, A., Isaia, R., Neri, A., Vitale, S., Aspinall, W. P., Bisson, M., et al. (2015), Quantifying volcanic hazard at Campi Flegrei caldera (Italy) with uncertainty assessment: I. Vent opening maps. *J. Geophys. Res. - Solid Earth*, 120, 2309–2329. doi: 10.1002/2014JB011775

Bevilacqua, A., Flandoli, F., Neri, A., Isaia, R., & Vitale, S. (2016), Temporal models for the episodic volcanism of Campi Flegrei caldera (Italy) with uncertainty quantification *J. Geophys. Res. - Solid Earth*, 121, 7821–7845. doi: 10.1002/2016JB013171

Bevilacqua, A., A. Neri, M. Bisson, T. Esposti Ongaro, F. Flandoli, R. Isaia, M. Rosi, S. Vitale (2017), Effects of vent location, event scale and time forecasts on pyroclastic density currents hazard maps at Campi Flegrei caldera, (Italy), *Front in Earth Sci* 5, 72, 1-16, doi: 10.3389/feart.2017.00072.

Bevilacqua, A., Bursik, M., Patra, A., Pitman, E. B., Yang, Q., Sangani, R., & Kobs-Nawotniak, S. (2018), Late Quaternary eruption record and probability of future volcanic eruptions in the Long Valley volcanic region (CA, USA). *J. Geophys. Res. - Solid Earth*, 123, 5466–5494. doi: 10.1029/2018JB015644

Bevilacqua A., Bertagnini A., Pompilio, M., Landi, P., Del Carlo, P., D Roberto, A., Piccione, C., Neri, A. (2020a), Historical catalog of major explosions and paroxysms at Stromboli (Italy). *INGV Ufficio Dati*, doi: 10.13127/STROMBOLI/STRCATALOG.

Bevilacqua A., A. Bertagnini, M. Pompilio, P. Landi, P. Del Carlo, A. Di Roberto, W. Aspinall, and A. Neri, (2020b). Major explosions and paroxysms at Stromboli (Italy): a new historical catalog and temporal models of occurrence with uncertainty quantification. *Sci Rep*, 10, 17357. doi: 10.1038/s41598-020-74301-8.

Bevilacqua A., Bertagnini A., Pompilio, M., Landi, P., Del Carlo, P., D Roberto, A., Piccione, C., Falsaperla, S., Spampinato, S., Neri, A. (2023), Catalog of major explosions and paroxysms at Stromboli volcano (Italy) from 1970 to 2023. *INGV Ufficio Dati*, doi: 10.13127/STROMBOLI/STRCATALOG2.

Bevilacqua, A., Nannipieri, L., Favalli, M., Fornaciai, A. (2024), UAS-based mapping of the July 3, 2019, ballistics density distribution on the W flank of Stromboli with uncertainty quantification. *Bull Volcanol,* 86, 48, doi: 10.1007/s00445-024-01741-9.

Bevilacqua, A., Neri, A., Landi, P., Del Carlo, P., Pompilio, M. (submitted), Ballistic projectile hazard of major explosions and paroxysms at Stromboli (Italy) with uncertainty quantification: 2. Conditional and temporal probability maps, doi: 10.5194/egusphere-2025-6540.

Bisson, M., Spinetti, C., Gianardi, R., Strehlow, K., De Beni, E., Landi, P. (2023), High-resolution mapping and dispersion analyses of volcanic ballistics emitted during the 3rd July 2019 paroxysm at Stromboli. *Sci Rep* 13:13465.

Blong, R. J. (1984), Volcanic hazards: a sourcebook on the effects of eruptions. *Academic Press*, Orlando.

Breard, E.C.P., Lube, G., Cronin, S.J., Fitzgerald, R., Kennedy, B., Scheu, B., Montanaro, C., White, J.D.L., Tost, M., Procter, J.N., Moebis, A. (2014), Using the spatial distribution and lithology of ballistic blocks to interpret eruption sequence and dynamics: August 6 2012 Upper Te Maari eruption, New Zealand, *J Volcanol Geoth Res* 276, 383-376.

Brown, S. K., Jenkins, S. F., Stephen, R., Sparks, J., Odbert, H., Auker, M. R. (2017), Volcanic fatalities database: analysis of volcanic threat with distance and victim classification. *J Appl Volcanol*, 6, 15, doi: 10.1186/s13617-017-0067-4.

https://doi.org/10.5194/egusphere-2025-6539
Preprint. Discussion started: 12 January 2026

Calvari, S., Giudicepietro, F., Di Traglia, F., Bonaccorso, A., Macedonio, G., Casagli, N. (2021), Variable Magnitude and Intensity of Strombolian Explosions: Focus on the Eruptive Processes for a First Classification Scheme for Stromboli Volcano (Italy), *Remote Sensing* 13, (5): 944. doi: 10.3390/rs13050944.

Calvari, S.; Nunnari, G. Statistical Insights on the Eruptive Activity at Stromboli Volcano (Italy) Recorded from 1879 to 2023. *Remote Sens* 15, 4822. doi: 10.3390/rs15194822.

Civico, R., Ricci, T., Scarlato, P., Andronico, D., Cantarero, M., Carr, B. B., De Beni, E., Del Bello, E., Johnson, J. B., Kueppers, U., Pizzimenti, L., Schmid, M., Strehlow, K., & Taddeucci, J. (2021). Unoccupied Aircraft Systems (UASs) Reveal the Morphological Changes at Stromboli Volcano (Italy) before, between, and after the 3 July and 28 August 2019 Paroxysmal Eruptions. *Remote Sensing* 13(15), 2870. doi: 10.3390/rs13152870.

Civico, R., Ricci, T., Cecili, A. et al. High-resolution topography reveals morphological changes of Stromboli volcano following the July 2024 eruption. *Sci Data* 11, 1219 (2024). doi: 10.1038/s41597-024-04098-y.

Coltelli, M., Del Carlo, P., and Pompilio, M. (2000). Vulcano and Stromboli, 1. Eruptive History (Stromboli), *Acta Vulcanol* 12, 93-95.

de' Michieli Vitturi, M., A. Neri, T. Esposti Ongaro, S. Lo Savio, and E. Boschi (2010), Lagrangian modeling of large volcanic particles: Application to Vulcanian explosions, *J Geophys Res* 115, B08206, doi: 10.1029/2009JB007111.

Di Lieto, B., Romano, P., Scarpa, R., and Linde, A. T. (2020), Strain signals before and during paroxysmal activity at Stromboli volcano, Italy. *Geophys Res Lett* 47 (21), e2020GL088521. doi:10.1029/2020GL088521.

Falsaperla, S., and Spampinato, S. (2003). Seismic insight into explosive paroxysms at Stromboli volcano, Italy, *J Volcanol Geoth Res* 125, 1–2, doi: 10.1016/S0377-0273(03)00093-3.

Fitzgerald, R. H., Tsunematsu, K., Kennedy, B. M., Breard, E. C. P., Lube, G., Wilson, T. M., Jolly, A. D., Pawson, J., Rosenberg, M. D., Cronin, S. J. (2014), The application of a calibrated 3D ballistic trajectory model to ballistic hazard assessments at Upper TeMaari, Tongariro. *J Volcanol Geoth Res*, 286:248–262.

Fitzgerald, R. H., Kennedy, B. M., Wilson, T. M., Leonard, G. S., Tsunematsu, K., Keys, H. (2018), The communication and risk management of volcanic ballistic hazards. In: *Observing the Volcano World, Volcano Crisis Communication*. Fearnley, C. J., Bird, D. K., Haynes, K., McGuire, W. J., Jolly, G. (Eds), Springer Open. *Advs in Volcanology*, 121–147.

Giordano, G., and De Astis, G. (2021). The summer 2019 basaltic Vulcanian eruptions (paroxysms) of Stromboli. *Bull Volcanol* 83, 1-27, doi: 10.1007/s00445-020-01423-2.

Graettinger, A. H., G. A. Valentine, I. Sonder, P.-S. Ross, J. D. L. White, and J. Taddeucci (2014), Maar-diatreme geometry and deposits: Subsurface blast experiments with variable explosion depth, *Geochem Geophys Geosyst* 15, 740–764, doi: 10.1002/2013GC005198.

Gurioli, L., Harris, A. J. L., Colo, L., Bernard, J., Favalli, M., Ripepe, M., Andronico, D. (2013), Classification, landing distribution, and associated flight parameters for a bomb field emplaced during a single major explosion at Stromboli, Italy. *Geology* 41(5):559–562.

Iezzi, A. M., Buzard, R. M., Fee, D., Matoza, R. S., Gestrich, J. E., Jolly, A. D., et al. (2023). UAS-based observations of infrasound directionality at Stromboli volcano, Italy. Geophysical Research Letters, 50, e2023GL102905. https://doi.org/10.1029/2023GL102905

https://doi.org/10.5194/egusphere-2025-6539
Preprint. Discussion started: 12 January 2026

Imbò, G. (1928): Parossismo di Stromboli nel settembre 1930. *Bull Volcanol* 15-18, 177-185.

Jaquet, O. & Carniel, R. (2003). Multivariate stochastic modeling: Towards forecasts of paroxysmal phases at Stromboli. *J Volcanol Geoth Res* 128, 261–271.

Maeno, F., Nakada, S., Nagai, M., Kozono, T. (2013), Ballistic ejecta and eruption condition of the vulcanian explosion of Shinmoedake volcano, Kyushu, Japan on 1 February, 2011, *Earth Planets Space* 65, 609–621.

Marzocchi, W.,&Bebbington, M. S. (2012). Probabilistic eruption forecasting at shortandlong time scales. *Bull Volcanol* 74, 1777–1805.

Massaro, S., Rossi, E., Sandri, L., Bonadonna, C., Selva, J., Moretti, R., Komorowski, J.C. (2022), Assessing hazard and potential impact associated with volcanic ballistic projectiles: The example of La Soufrière de Guadeloupe volcano (Lesser Antilles), *J Volcanol Geoth Res* 423, 107473.Neri, A., A. Bevilacqua, T. Esposti Ongaro, R. Isaia, W.P. Aspinall, M. Bisson, F. Flandoli, P. J. Baxter, A. Bertagnini, E. Iannuzzi, S. Orsucci, M. Pistolesi, M. Rosi, and S. Vitale (2015), Quantifying volcanic hazard at Campi Flegrei caldera (Italy) with uncertainty assessment: II. Pyroclastic density current invasion maps, *J Geophys Res – Solid Earth* 120, 2330-2349, doi: 10.1002/2014JB011776.

Mercalli (1883). I vulcani ed i fenomeni vulcanici in Italia. Lo Stromboli. In: "Geologia d'Italia", Vallardi, Milano, 135-144.

Neri, A., A. Bevilacqua, T. Esposti Ongaro, R. Isaia, W.P. Aspinall, M. Bisson, F. Flandoli, P. J. Baxter, A. Bertagnini, E. Iannuzzi, S. Orsucci, M. Pistolesi, M. Rosi, and S. Vitale (2015), Quantifying volcanic hazard at Campi Flegrei caldera (Italy) with uncertainty assessment: II. Pyroclastic density current invasion maps, *Journal of Geophysical Research – Solid Earth*, 120, 2330-2349, doi: 10.1002/2014JB011776.

Pistolesi, M., Rosi, M., Pioli, L., Renzulli, A., Bertagnini, A. and Andronico, D. (2008). The Paroxysmal Event and Its Deposits. In The Stromboli Volcano: An Integrated Study of the 2002–2003 Eruption (eds. S. Calvari, S. Inguaggiato, G. Puglisi, M. Ripepe and M. Rosi), *Geophysical Monograph Series AGU*, doi: 10.1029/182GM26.

Pistolesi, M., D. Delle Donne, L. Pioli, M. Rosi, and M. Ripepe (2011), The 15 March 2007 explosive crisis at Stromboli volcano, Italy: Assessing physical parameters through a multidisciplinary approach, *J Geophys Res* 116, B12206, doi: 10.1029/2011JB008527.

Platania, G., (1922), L'esplosione dello Stromboli del maggio 1919. *Boll. Accad. Gioenia Sci. Nat. Catania*, 50, 1-17.

Pompilio, M., Bertagnini, A., Di Roberto, A. (2010) Present-day activity of Stromboli: eruptive history and eruptive styles, *Acta Vulcanol* 22 (1-2), 29-34.

Ponte, G. (1916). Lo Stromboli dopo il parossismo del 1915. *R Accad Naz Lincei* 25, 373-377.

Ponte, G. (1919), La catastrofica esplosione dello Stromboli. *R. Accad. Naz. Lincei*, 28, 89-94.

Ponte, G. (1924), Stato attuale dei vulcani italiani. *Riv Ita Vulc* 1, 32-35.

Ranfaldi, F. (1921), Sull'eruzione dello Stromboli del 22 maggio 1919 e sui fenomeni vulcanici in generale. *Atti Reale Accad Peloritana* 29, 3-57.

Riccò, A. (1907). Attività dello Stromboli, *Boll Accad Gioenia Sci Nat Catania* 19, 7-12.

https://doi.org/10.5194/egusphere-2025-6539
Preprint. Discussion started: 12 January 2026

Richardson, J. A., Wilson, J. A., Connor, C. B., Bleacher, J. E., & Kiyosugi, K. (2017). Recurrence rate and magma effusion rate for the latest volcanism on Arsia Mons, Mars. *Earth Planet Sci Lett* 458, 170–178.

Ripepe, M., Lacanna, G., Pistolesi, M., Silengo, M. C., Aiuppa, A., Laiolo, M., Massimetti, F., Innocenti, L., Della Schiava, M., Bitetto, M., La Monica, F. P., Nishimura, T., Rosi, M., Mangione, D., Ricciardi, A., Genco, R., Coppola, D.,Marchetti, E., Delle Donne, D. (2021), Ground deformation reveals the scale-invariant conduit dynamics driving explosive basaltic eruptions. *Nat Comm* 12, 1683, doi: 10.1038/s41467-021-21722-2.

Rittmann, A. (1931): Der Ausbruch des Stromboli am 11 September 1930. *Zeits Vulkanol* 14, 47-77.

Rittmann, A. (1933): Beitrag zur Kenntnis des Strombolikraters. *Zeits Vulkanol* 15, 184-190.

Rosi, M., Bertagnini, A., Harris, A. J. L., Pioli, L., Pistolesi, M., and Ripepe, M. (2006). A case history of paroxysmal explosion at Stromboli: timing and dynamics of the April 5, 2003 event. *Earth Planet Sci Lett* 243, 594-606, doi: 10.1016/j.epsl.2006.01.035.

Rosi, M., Pistolesi, M., Bertagnini, A., Landi, P., Pompilio, M., Di Roberto, R. (2013), Stromboli volcano, Aeolian Islands (Italy): present eruptive activity and hazards. In: Lucchi, F., Peccerillo, A., Keller, J., Tranne, C. A., Rossi, P. L. (eds) 2013. *The Aeolian Islands Volcanoes*. *Geological Society, London, Memoirs*, 37, 473–490. http://dx.doi.org/10.1144/M37.14. The Geological Society of London, 2013.

Rutarindwa, R., Spiller, E. T., Bevilacqua, A., Bursik, M. I., & Patra, A. K. (2019). Dynamic probabilistic hazard mapping in the Long Valley Volcanic Region CA: Integrating vent opening maps and statistical surrogates of physical models of pyroclastic density currents. *J Geophys Res Solid Earth* 124. doi: 10.1029/2019JB017352.

Schmid, M., Kueppers, U., Civico, R., Ricci, T., Taddeucci, J. and Dingwell, D. B. (2021) Characterising vent and crater shape changes at Stromboli: implications for risk areas, *Volcanica*, 4(1), p. 87–105. doi: 10.30909/vol.04.01.87105.

Sonder, I., A. H. Graettinger, and G. A. Valentine (2015), Scalingmultiblast craters: generalapproach and application tovolcanic craters, *J Geophys Res Solid Earth* 120, 6141–6158, doi: 10.1002/2015JB012018.

Sonder, I., Graettinger, A., Neilsen, T. B., Matoza, R. S., Taddeucci, J., Oppenheimer, J., et al. (2022). Experimental multiblast craters and ejecta—seismo-acoustics, jet characteristics, craters, and ejecta deposits and implications for volcanic explosions. *J Geophys Res Solid Earth* 127, e2022JB023952. doi: 10.1029/2022JB023952.

Sparks, R. S. J., & Aspinall, W. A. (2004). Volcanic activity: Frontiers and challenges in forecasting, prediction and risk assessment, in: The state of the planet, Frontiers and challenges in geophysics, *Geophysical Monograph 150*, IUGG, 19, 359–373.

Taddeucci, J., G. A. Valentine, I. Sonder, J. D. L. White, P. S. Ross, and P. Scarlato (2013), The effect of pre-existing craters on the initial development of explosive volcanic eruptions: An experimental investigation, *Geophys Res Lett* 40, 507–510, doi: 10.1002/grl.50176.

Taddeucci, J., Alatorre-Ibargüengoitia, M.A., Cruz-Vàzquez, O., Del Bello, E., Scarlato, P., Ricci, T. (2017), In-flight dynamics of volcanic ballistic projectiles. *Rev of Geophys* 55 675-718. Doi: 10.1002/2017RG000564

Tadini, A., Azzaoui, N., Roche, O., Samaniego, P., Bernard, B., Bevilacqua, A., Hidalgo, S., Guillin, A., Gouhier, M. (2022). Tephra fallout probabilistic hazard maps for Cotopaxi and Guagua Pichincha volcanoes (Ecuador) with uncertainty quantification. *J Geophys Res Solid Earth* 127, e2021JB022780. doi: 10.1029/2021JB022780.

https://doi.org/10.5194/egusphere-2025-6539
Preprint. Discussion started: 12 January 2026

Tsunematsu, K., Chopard, B., Falcone, J.L., Bonadonna, C. (2015), A numerical model of ballistic transport with collisions in a volcanic setting, *Comput & Geosci* 63, 62-69, doi: 10.1016/j.cageo.2013.10.016.

Tsunematsu, K., Ishimine, Y., Kaneko, T., Yoshimoto, M., Fujii, T., Yamaoka, K. (2016), Estimation of ballistic block landing energy during 2014 Mount Ontakeeruption. *Earth, Planets Space* 68:88.

Valentine, G. A., J. D. L. White, P.-S. Ross, J. Amin, J. Taddeucci, I. Sonder, and P. J. Johnson (2012), Experimental craters formed by single and multiple buried explosions and implications for volcanic craters with emphasis on maars, *Geophys Res Lett* 39, L20301, doi: 10.1029/2012GL053716.

Valentine, G. A., A. H. Graettinger, and I. Sonder (2014), Explosion depths for phreatomagmatic eruptions, *Geophys Res Lett* 41, 3045–3051, doi: 10.1002/2014GL060096.

Valentine, G.A., Graettinger, A.H., Macorps, É., Ross, P., White, J., Doring, E., Sonder, I. (2015), Experiments with vertically and laterally migrating subsurface explosions with applications to the geology of phreatomagmatic and hydrothermal explosion craters and diatremes. *Bull Volcanol* 77, 15. doi: 10.1007/s00445-015-0901-7.

Vanderkluysen, L., Harris, A.J.L., Kelfoun, K. et al. Bombs behaving badly: unexpected trajectories and cooling of volcanic projectiles. *Bull Volcanol* 74, 1849–1858 (2012). doi: 10.1007/s00445-012-0635-8.

Voloschina, M., Métrich, N., Bertagnini, A., Marianelli, P., Aiuppa, A., Ripepe, M., Pistolesi, M. (2023), Explosive eruptions at Stromboli volcano (Italy): a comprehensive geochemical view on magma sources and intensity range. *Bull Volcanol* 85, 34, doi: 10.1007/s00445-023-01647-y

Watson, E. J., Swindles, G. T., Savov, I. P., Lawson, I. T., Connor, C. B., & Wilson, J. A. (2017). Estimating the frequency of volcanic ash clouds over northern Europe. *Earth Planet Sci Lett* 460, 41–49.

Yamaoka, K., Geshi, N., Hashimoto, T., Ingebritsen, S. E., Oikawa, T. (2016), Special issue “The phreatic eruption of Mt. Ontake volcano in 2014” - (Preface). *Earth, Planets and Space* (2016) 68, 175. doi: 10.1186/s40623-016-0548-4.

Zuccarello, L., Gheri, D., De Angelis, S., Civico, R., Ricci, T., and Scarlato, P. (2025): Geophysical fingerprint of the 4-11 July 2024 eruptive activity at Stromboli volcano, Italy, *Nat Hazards Earth Syst Sci* 25, 2317–2330, doi: 10.5194/nhess-25-2317-2025.

References from Supporting Information

Abbruzzese, D. (1935). Attività dello Stromboli dal 1930 al 1934. *Boll Soc Sism It* 33, 118-125.

Abbruzzese, D. (1936a). Sulla catastrofica esplosione dello Stromboli dell'11 settembre del 1930. *Atti Accad Gioenia Sc Nat Catania* 1, 1-33.

Abbruzzese, D. (1936b). Notizie Vulcanologiche. *Boll Soc Sism It* 34, 78-79.

Abbruzzese, D. (1937a). Attività dello Stromboli dal 1934 al 1936. *Boll Vulcanol* 2, 70-76.

Abbruzzese, D. (1937b). Notizie Vulcanologiche. *Boll Soc Sism It* 35, 70-73.

Abbruzzese, D. (1938). Notizie Vulcanologiche. *Boll Soc Sism It* 36, 65.

Abbruzzese, D. (1939). Notizie Vulcanologiche. *Boll Soc Sism It* 37, 198-199.

https://doi.org/10.5194/egusphere-2025-6539
Preprint. Discussion started: 12 January 2026

Abbruzzese, D. (1940). Attività dello Stromboli dal 1937 al giugno del 1939. *Boll Volcanol* 7, 57-66.

Anderson, T. (1905). On Certain Recent Changes in the Crater of Stromboli. *Geograph J 25*, 123-129.

Andronico, D., and Pistolesi, M. (2010). The November 2009 paroxysmal explosions at Stromboli. *J Volcanol Geoth Res* 196, 120-125, doi: 10.1016/j.jvolgeores.2010.06.005.

Andronico, D., Taddeucci, J., Cristaldi, A., Miraglia, L., Scarlato, P., and Gaeta, M. (2013). The 15 March 2007 paroxysm of Stromboli: video-image analysis, and textural and compositional features of the erupted deposit. *Bull Volc* 75, 1-19, doi: 10.1029/2011JB008527.

Andronico, D., Del Bello, E., D'Oriano, C., Landi, P., Pardini, F., Scarlato, P., de' Michieli Vitturi, M., Taddeucci, J., Cristaldi, A., Ciancitto, F., Pennacchia, F., Ricci, T., and Valentini, F. (2021). Uncovering the eruptive patterns of the 2019 double paroxysm eruption crisis of Stromboli volcano. *Nature Communications* 12(1), 4213, doi: 10.1038/s41467-021-24420-1.

Arcidiacono, S. (1895a). Rassegna dei principali fenomeni eruttivi avvenuti in Sicilia e nelle isole adiacenti, durante il quadrimestre gennaio-aprile 1895. *Boll Soc Sism It* 1, 78-81.

Arcidiacono, S. (1895b). Rassegna dei principali fenomeni eruttivi avvenuti in Sicilia e nelle isole adiacenti, durante il quadrimestre maggio-agosto 1895. *Boll Soc Sism It* 1, 153-156.

Arcidiacono, S. (1895c). Rassegna dei principali fenomeni eruttivi avvenuti in Sicilia e nelle isole adiacenti durante il quadrimestre settembre-dicembre 1895. *Boll Soc Sism It* 1, 157-159.

Arcidiacono, S. (1896a). Rassegna dei principali fenomeni eruttivi avvenuti in Sicilia e nelle isole adiacenti, durante il semestre gennaio-giugno 1896. *Boll Soc Sism It* 2, 122-124.

Arcidiacono, S. (1896b). Rassegna dei principali fenomeni eruttivi avvenuti in Sicilia e nelle isole adiacenti durante il semestre luglio-dicembre 1896. *Boll Soc Sism It* 2, 229-232.

Arcidiacono, S. (1897a). Rassegna dei principali fenomeni eruttivi avvenuti in Sicilia e nelle isole adiacenti, durante il 1° semestre gennaio-giugno 1897. *Boll Soc Sism It* 3, 57-60.

Arcidiacono, S. (1897b). Principali fenomeni eruttivi avvenuti in Sicilia e nelle isole adiacenti, durante il semestre Luglio-Dicembre 1897. *Boll Soc Sism It* 3, 203-213.

Arcidiacono, S. (1898a). Principali fenomeni eruttivi avvenuti in Sicilia e nelle isole adiacenti nel semestre gennaio-giugno, 1898. *Boll Soc Sism It* 4, 107-113.

Arcidiacono, S. (1898b). Principali fenomeni eruttivi avvenuti in Sicilia e nelle isole adiacenti nel semestre luglio-dicembre, 1898. *Boll Soc Sism It* 4, 261-275.

Arcidiacono, S. (1900). Principali fenomeni eruttivi avvenuti in Sicilia e nelle isole adiacenti nell'anno 1899. *Boll Soc Sism It* 6, 101-114.

Arcidiacono, S. (1901). Principali fenomeni eruttivi avvenuti in Sicilia e nelle isole adiacenti durante l'anno 1900. *Boll Soc Sism It* 7, 82-91.

Arcidiacono, S. (1904). Principali fenomeni eruttivi avvenuti in Sicilia e nelle isole adiacenti durante l'anno 1901. *Boll Soc Sism It* 10, 65-71.

Arcidiacono, S. (1906). Principali fenomeni eruttivi avvenuti in Sicilia e nelle isole adiacenti durante l'anno 1902. *Boll Soc Sism It* 11, 45-53.

Asburgo, L.S. (1896). Die Liparischen Inseln, Siebentes Heft: Stromboli. 51p. Prag. Druck Und Verlag Von Heinr. Mercy.

Barberi, F., Civetta, L., Rosi, M., and Scandone, R. (2009). Chronology of the 2007 eruption of Stromboli and the activity of the Scientific Synthesis Group. *J Volcanol Geoth Res* 182(3-4), 123-130, doi: 10.1016/j.jvolgeores.2008.09.019.

Barberi, F., Rosi, M., and Sodi, A. (1993). Volcanic hazard assessment at Stromboli based on a review of historical data. *Acta Vulc* 3, 173-187.

Bertagnini, A., Coltelli, M., Landi, P., Pompilio, M., and Rosi, M. (1999). Violent explosions yield new insights into dynamics of Stromboli volcano. *Eos Transactions American Geophysical Union* 80(52), 633-636, doi: 10.1029/99EO00415

https://doi.org/10.5194/egusphere-2025-6539
Preprint. Discussion started: 12 January 2026

Bevilacqua, A., Bertagnini, A., Pompilio, M., Landi, P., Del Carlo, P., Di Roberto, A., Aspinall, W., Neri, A. (2020). Major explosions and paroxysms at Stromboli (Italy): a new historical catalog and temporal models of occurrence with uncertainty quantification. *Scientific Reports* 10, 17357. doi: 10.1038/s41598-020-74301-8

Bisson, M., Spinetti, C., Gianardi, R. et al. High-resolution mapping and dispersion analyses of volcanic ballistics emitted during the 3rd July 2019 paroxysm at Stromboli. *Scientific Reports* 13, 13465 (2023). doi: 10.1038/s41598-023-39600-w

Calvari, S., Giudicepietro, F., Di Traglia, F., Bonaccorso, A., Macedonio, G., Casagli, N. (2021). Variable Magnitude and Intensity of Strombolian Explosions: Focus on the Eruptive Processes for a First Classification Scheme for Stromboli Volcano (Italy). *Remote Sens* 13, 944. doi: 10.3390/rs13050944.

Calvari, S., Bonaccorso, A., Madonia, P., Neri, M., Liuzzo, M., Salerno, G. G., Behncke, B., Caltabiano, T., Cristaldi, A., Giuffrida, G., La Spina, A., Marotta, E., Ricci, T., and Spampinato, L. (2014). Major eruptive style changes induced by structural modifications of a shallow conduit system: the 2007–2012 Stromboli case. *Bull Volc* 76, 1-15, doi: doi: 10.1007/s00445-014-0841-7.

Calvari, S., Spampinato, L., and Lodato, L. (2006). The 5 April 2003 vulcanian paroxysmal explosion at Stromboli volcano (Italy) from field observations and thermal data. *J Volcanol Geoth Res* 149(1-2), 160-175.

Calvari, S., Bonaccorso, A., Cappello, A., Giudicepietro, F., and Sansosti, E. (2022). Volcanic Processes Monitoring and Hazard Assessment Using Integration of Remote Sensing and Ground-Based Techniques. *Remote Sensing* 14(15), 3626, doi: doi: 10.3390/rs14153626.Cavallaro, C. (1957a). L'attività dello Stromboli dal 1940 al 1953. *Boll Accad Gioenia Sci Nat Catania* 3, 525-532.

Cavallaro, C. (1957b). L'attività dello Stromboli dall'aprile 1956 al 31 dicembre 1956. *Boll Acc Gioenia Sci Nat Catania* 4, 103-118.

Cavallaro, C. (1962). L'esplosione dello Stromboli dell'11 Luglio 1959. *Riv Stromboli* 8, 11-14.

Cavallaro, C. (1967). Le attività dello Stromboli nel triennio 1957-59 e le variazioni morfologiche da esse determinate, *Atti del XX Congresso Geografico Italiano Roma*. 29 Marzo - 3 Aprile 1967, 1-15.

Christa, E. (1925). Beobachtungen am Stromboli Ende April 1924. *Zeits Vulkanol* 10, 1-4.

Coltelli, M., Del Carlo, P., and Pompilio, M. (2000). Vulcano and Stromboli, 1. Eruptive History (Stromboli), *Acta Vulc* 12, 93-95.

Coltelli, M., and Cardaci, C. (1994). Stromboli, in Italian volcanic activity during 1991-1994, by Barberi, F., Bertagnini, A., Landi, P., *Suppl Boll Geofisica Teo Appl* 36, 679-683.

Cucuzza Silvestri, S. (1955). La recente attività dello Stromboli (gennaio-marzo 1954). *Boll Accad Gioenia Sci Nat Catania* 3. 16-32.

De Fiore, 0. (1915). I fenomeni eruttivi avvenuti allo Stromboli dal 1909 al 1914 ed il loro meccanismo. *Zeits Vulkanol* 1. 225-246.

De Fiore, 0. (1923). I fenomeni eruttivi avvenuti allo Stromboli dal 1914 al 1916. *Boll Soc Sism It* 24. 9-66.

De Rossi, M.S. (1880). Quadri sinottici e cronologici dei fenomeni endogeni italiani. *Bull Vulc Ita* 7, 169-174.

De Rossi, M.S. (1882). Corrispondenza per le notizie e le descrizioni dei fenomeni. *Bull Vulc Ita* 9, 200-203.

Eredia, F. (1924). Lo Stromboli nelle recenti eruzioni vulcaniche. *Secolo* XX, 4p.

Falsaperla, S. (1991). Stromboli, in Data related to eruptive activity, unrest phenomena and other observations on the Italian active volcanoes 1990*, Acta Vulc* 1, 272-274.

Falsaperla, S., and Villari, L. (1991). Stromboli, in Volcanological research in Italy (1987-1990), by Barberi F., Neri G., Valenza M., and Villari L., *Suppl Boll Geofisica Teo Appl* 32, 424-427.

Falsaperla, S., Montalto, A., and Spampinato, S. (1994). Seismic investigations on volcanic tremor at Stromboli volcano (Italy), *Acta Vulc* 5, 179-186.

Falsaperla, S., and Cardaci, C. (1994). Seismic activity at Stromboli volcano, *Acta Vulc* 6, 56-58.

Falsaperla, S., and Cardaci, C. (1998). Main features of seismic activity at Stromboli, *Acta Vulc* 10, 136-139.

Falsaperla, S., and Spampinato, S. (2003). Seismic insight into explosive paroxysms at Stromboli volcano, Italy, *J Volcanol Geoth Res* 125, 1–2, doi: 10.1016/S0377-0273(03)00093-3.

Giordano, G., and De Astis, G. (2021). The summer 2019 basaltic Vulcanian eruptions (paroxysms) of Stromboli. *Bull Volc* 83, 1-27, doi: 10.1007/s00445-020-01423-2.

https://doi.org/10.5194/egusphere-2025-6539
Preprint. Discussion started: 12 January 2026

Giudicepietro, F., Calvari, S., Alparone, S., Bianco, F., Bonaccorso, A., Bruno, V., Caputo, T., Cristaldi, C., D'Auria, L., De Cesare, W., Di Lieto, B., Esposito, A. M., Gambino, S., Inguaggiato, S., Macedonio, G., Martini, M., Mattia, M., Orazi, M., Paonita, A., Peluso, R., Privitera, E., Romano, P., Scarpato, G., Tramelli, A., and Vita, F. (2019). Integration of ground-based remote-sensing and in situ multidisciplinary monitoring data to analyze the eruptive activity of Stromboli volcano in 2017–2018. *Remote Sensing* 11(15), 1813, doi: 10.3390/rs11151813.

Gurioli, L., Harris, A. J. L., Colò, L., Bernard, J., Favalli, M., Ripepe, M., and Andronico, D. (2013). Classification, landing distribution, and associated flight parameters for a bomb field emplaced during a single major explosion at Stromboli, Italy. *Geology* 41(5), 559-562, doi: 10.1130/G33967.1.

Hantke, G. (1951). Ubersicht uber die vulkanische Tatigkeit 1948-1950. *Bull Volcanol* 11, 179-180.

Hantke, G. (1955). Ubersicht uber die vulkanische Tatigkeit 1951-1953. *Bull Volcanol* 14, 107-109.

Hantke, G. (1959). Ubersicht uber die vulkanische Tatigkeit 1954-1956. *Bull Volcanol* 20 27-29.

Hantke, G. (1962). Ubersicht uber die vulkanische Tatigkeit 1957-1959. *Bull Volcanol* 24, 344-345.

Imbò, G. (1928): Parossismo di Stromboli nel settembre 1930. *Bull Volcanol* 15-18, 177-185.

Imbò, G. (1935). Considerazioni sull'attività dello Stromboli successiva al parossismo del settembre 1930. *Ann Reale Oss Ves* 3, 3-15.

Insinga, L., Voloschina, M., Marianelli, P. et al. Magma source, pre-eruptive dynamics and timescales of major explosions at Stromboli volcano (Italy). Bull Volcanol 87, 75 (2025). https://doi.org/10.1007/s00445-025-01862-9.

La Felice, S., and Landi, P. (2011). The 2009 paroxysmal explosions at Stromboli (Italy): magma mixing and eruption dynamics. *Bull Volc* 73, 1147-1154, doi: 10.1007/s00445-011-0502-z.

Landi, P., D'Oriano, C., Petrelli, M., Nazzari, M., and Andronico, D. (2022). Inferences on the magmatic plumbing system at Stromboli volcano (Italy) from trace element geochemistry of matrix glasses and minerals in different types of explosive eruptions. *Contrib Mineral Petrol* 177, 96. doi: 10.1007/s00410-022-01962-1

Landi, P., Métrich, N., Bertagnini, A., and Rosi, M. (2008). Recycling and "re-hydration" of degassed magma inducing transient dissolution/crystallization events at Stromboli (Italy). *J Geoph Res Solid Earth* 174(4), 325-336, doi: 10.1016/j.jvolgeores.2008.02.013.

Langer, H., and Falsaperla, S. (1996). Long-term observation of volcanic tremor on Stromboli volcano (Italy): a synopsis, *Pageoph* 147, 57–82 (1996). doi: 10.1007/BF00876436.

Losacco U., (1973). Saggio sulla toponomastica delle Isole Eolie, *L'Universo*, anno LIII. Firenze, I.G.M., pp.381-446

Malladra, E. (1922). Etna, Vulcano, Stromboli nell'estate 1921. Giannini, Napoli, 64 pp.

Martini M, Giudicepietro F, D'Auria L, Esposito AM, Caputo T, Curciotti R, De Cesare W, Orazi M, Scarpato G, Caputo A. Seismological monitoring of the February 2007 effusive eruption of the Stromboli volcano. *Ann Geophys* 50, 775-788, doi: 10.4401/ag-3056.

Mercalli, G. (1879). Corrispondenza: Eruzioni dello Stromboli. *Bull Vulc Ita* 6, 96-97.

Mercalli, G. (1881). Natura delle eruzioni dello Stromboli ed in generale dell'attivita sismo-vuJcanica delle Isole Eoiie. *Atti Soc It Sc Nat* 24, 105-134.

Mercalli, G. (1882). Corrispondenza: Eruzione dello Stromboli ai 18 Ottobre. *Bull Vulc Ita* 9, 25-26.

Mercalli, G. (1884). Notizie sullo stato attuale dei Vulcani attivi italiani. *Atti Soc It Sc Nat* 27, 184-199.

Mercalli, G. (1886). La Fossa di Vulcano e lo Stromboli dal 1884 al 1886. *Atti Soc It Sc Nat* 29, 352-361.

Mercalli, G. (1888a). L'isola di Vulcano e lo Stromboli dal 1886 al 1888. *Atti Soc It Sc Nat* 31, 407-411.

Mercalli, G. (1888b). Studio comparativo dei fenomeni vulcanici osservati nell'arcipelago eolico durante il periodo eruttivo di Vulcano. *Ann Uff Cent Meteor Geodinam It* 10, 177-186.

Nappi, G. (1975). Sull'attivita' recente dello Stromboli (ottobre 1972-dicembre 1974*). Boll Soc Geol It* 94 , 465-478.

Nappi, G. (1976a). Recent activity of Stromboli (November 5–24 1975). *Nature* 261, 119–120.

Nappi, G. (1976b). L'eruzione dello Stromboli del novembre 1975. *Boll Soc Geol It* 95 , 991-1008.

https://doi.org/10.5194/egusphere-2025-6539
Preprint. Discussion started: 12 January 2026

Perret, F. A. (1913): Report on the recent great eruption of the volcano Stromboli. *Smith Rep* 1912, 285-289.

Perret, F.A. (1916): The lava eruption of Stromboli summer-autumn, 1915. *Am J Sci* 42, 436-457.

Pichavant, M., Di Carlo, I., Pompilio, M., and Le Gall, N. (2022). Timescales and mechanisms of paroxysm initiation at Stromboli volcano, Aeolian Islands, Italy. *Bull Volc* 84(4), 36, doi: doi: 10.1007/s00445-022-01545-9.

Pistolesi, M., Rosi, M., Pioli, L., Renzulli, A., Bertagnini, A. and Andronico, D. (2008). The Paroxysmal Event and Its Deposits. In The Stromboli Volcano: An Integrated Study of the 2002–2003 Eruption (eds S. Calvari, S. Inguaggiato, G. Puglisi, M. Ripepe and M. Rosi), *Geophysical Monograph Series AGU*, doi: 10.1029/182GM26.

Pistolesi, M., Delle Donne, D., Pioli, L., Rosi, M., and Ripepe, M. (2011). The 15 March 2007 explosive crisis at Stromboli volcano, Italy: assessing physical parameters through a multidisciplinary approach. *J Geoph Res Solid Earth* 116(B12), doi: 10.1029/2011JB008527.

Platania, G. (1906). Stromboli. Mem. *CSR Acc Zelanti* 5, 1-11.

Platania, G. (1910). I fenomeni eruttivi dello Stromboli nella primavera del 1907. *Ann Uff Cent Meteor Geodinam It* 30, 1-27.

Platania, G. (1916). I fenomeni eruttivi dello Stromboli nel novembre 1915. *R Accad Naz Lincei* 25, 317-321.

Platania, G., (1922). L'esplosione dello Stromboli del maggio 1919. *Boll Accad Gioenia Sci Nat Catania* 50, 1-17.

Ponte, G. (1916). Lo Stromboli dopo il parossismo del 1915. *R Accad Naz Lincei* 25, 373-377.

Ponte, G. (1919). La catastrofica esplosione dello Stromboli. *R Accad Naz Lincei* 28, 89-94.

Ponte, G. (1921). La formidabile esplosione delio Stromboli del 1916. *Mem R Com Geol It* 7, 1-34.

Ponte, G. (1923). L'attività dello Stromboli nel 1922. *Boll Accad Gioenia Sci Nat Catania* 51, 1-5.

Ponte, G. (1924). Stato attuale dei vulcani italiani. *Riv Ita Vulc* 1, 32-35.

Ponte, G. (1948). Attività straordinaria dello Stromboli. *Ann Geofisica* 1, 200-202.

Ranfaldi, F. (1921). Sull'eruzione dello Stromboli del 22 maggio 1919 e sui fenomeni vulcanici in generale. Atti Reale Accad Peloritana 29, 3-57.

Riccò, A. (1907a). Sulla attività dello Stromboli dai 1891 in poi. *Boll Soc Sism It* 12, 183-205.

Riccò, A. (1907b). Attività dello Stromboli, *Boll Accad Gioenia Sci Nat Catania* 19, 7-12.

Riccò, A. (1916). Parossismo dello Stromboli del 1915. *Att Accad Naz Lincei* 25, 251-259.

Riccò, A. and Mercalli, G. (1892). Sopra il periodo eruttivo dello Stromboli cominciato ii 24 giugno 1891. *Ann Uff Cent Meteor Geodinam It* 11, 189-221.

Rittmann, A. (1931): Der Ausbruch des Stromboli am 11 September 1930. *Zeits Vulkanol* 14, 47-77.

Rittmann, A. (1933): Beitrag zur Kenntnis des Strombolikraters. *Zeits Vulkanol* 15, 184-190.

Rosi, M., Bertagnini, A., Harris, A. J. L., Pioli, L., Pistolesi, M., and Ripepe, M. (2006). A case history of paroxysmal explosion at Stromboli: timing and dynamics of the April 5, 2003 event. *Earth and Plan Sci Lett* 243(3-4), 594-606, doi: 10.1016/j.epsl.2006.01.035.

Rosi, M., and Sbrana, A. (1987). L'attività esplosiva del 6 dicembre 1985 dello Stromboli. *Rend Soc It Miner Petrol* 42, 313-313.

Rosi, M., Pistolesi, M., Bertagnini, A., Landi, P., Pompilio, M., and Di Roberto, A. (2013). Chapter 14 Stromboli volcano, Aeolian Islands (Italy): present eruptive activity and hazards. *Geological Society London Memoirs* 37(1), 473-490, doi: 10.1144/M37.1.

Schmid, M., Kueppers, U., Ricci, T., Civico, R., Cigala, V., Fee, D., Gestrich, J. E., Iezzi, A. M., Cimarelli, C., Vossen, C. E. J., Buzard, R. M., Ripepe, M., Lacanna, G. and Dingwell, D. B. (2025). The morphological response to the 13 May 2022 major explosive event at Stromboli volcano, Italy, characterised by high-resolution UAS surveys, Volcanica, 8(2), pp. 387–397. doi: 10.30909/vol/crjj4989.

Voloschina, M., Métrich, N., Bertagnini, A., Marianelli, P., Aiuppa, A., Ripepe, M., and Pistolesi, M. (2023). Explosive eruptions at Stromboli volcano (Italy): a comprehensive geochemical view on magma sources and intensity range. *Bull Volcanol* 85, 34 (2023). doi: 10.1007/s00445-023-01647-y